

SAGE-AMINE: GENERATIVE AMINE DESIGN WITH MULTI-PROPERTY OPTIMIZATION FOR EFFICIENT CO₂ CAPTURE

Hocheol Lim^{*a}, Hyein Cho^b, and Jeonghoon Kim^a

^aBioinformatics and Molecular Design Research Center (BMDRC), Incheon, 21983, Republic of Korea

^bThe Interdisciplinary Graduate Program in Integrative Biotechnology & Translational Medicine, Yonsei University, Incheon, 21983, Republic of Korea

March 5, 2025

* Corresponding author: Hocheol Lim (ihc0213@yonsei.ac.kr)

ABSTRACT

Efficient CO₂ capture is vital for mitigating climate change, with amine-based solvents being widely used due to their strong reactivity with CO₂. However, optimizing key properties such as basicity, viscosity, and absorption capacity remains challenging, as traditional methods rely on labor-intensive experimentation and predefined chemical databases, limiting the exploration of novel solutions. Here, SAGE-Amine was introduced, a generative modeling approach that integrates Scoring-Assisted Generative Exploration (SAGE) with quantitative structure-property relationship models to design new amines tailored for CO₂ capture. Unlike conventional virtual screening restricted to existing compounds, SAGE-Amine generates novel amines by leveraging autoregressive natural language processing models trained on amine datasets. SAGE-Amine identified known amines for CO₂ capture from scratch and successfully performed single-property optimization, increasing basicity or reducing viscosity or vapor pressure. Furthermore, it facilitated multi-property optimization, simultaneously achieving high basicity with low viscosity and vapor pressure. The 10 top-ranked amines were suggested using SAGE-Amine and their thermodynamic properties were further assessed using COSMO-RS simulations, confirming their potential for CO₂ capture. These results highlight the potential of generative modeling in accelerating the discovery of amine solvents and expanding the possibilities for industrial CO₂ capture applications.

Keywords Material discovery · De novo molecular design · Quantitative structure-property relationship · Solvent Design · Amine Design

1 Introduction

The rapid industrial development and increasing global energy demand have led to sustained reliance on fossil fuels, causing a significant rise in CO₂ emissions and disrupting the natural carbon cycle [1, 2]. These emissions are a major driver of the greenhouse effect and global warming, creating urgent environmental challenges. The natural capacity of oceans to absorb atmospheric CO₂ is insufficient to cope with these elevated emission levels [2], making additional mitigation strategies essential. Carbon capture and storage technologies have gained prominence, with amine-based solvents standing out for post-combustion CO₂ capture due to their compatibility with existing industrial processes [3, 4].

Amine-based solvents, such as monoethanolamine (MEA), diethanolamine (DEA), methyldiethanolamine (MDEA), and piperazine (PZ), have been extensively studied for post-combustion CO₂ capture [5–8]. These solvents react chemically with CO₂, forming reversible bonds that allow for efficient gas separation. Primary and secondary amines form carbamates upon reacting with CO₂, whereas tertiary amines capture CO₂ as bicarbonate [4]. The formation of

bicarbonate by tertiary amines requires a lower heat of reaction than carbamate formation, resulting in energy savings during regeneration [9]. However, these methods encounter economic and environmental challenges, including chemical degradation, corrosivity, toxicity, and high energy demands for solvent regeneration [10]. These drawbacks underscore the critical need for discovering new amines with enhanced properties to improve the efficiency and cost-effectiveness of CO₂ capture processes.

Recent research has aimed to improve these solvents by focusing on developing blends or novel amine formulations that offer a better balance between CO₂ absorption capacity, stability, and energy efficiency [3, 11]. While primary amines like MEA react quickly with CO₂, tertiary amines such as MDEA provide better regeneration efficiency but lower reactivity, leading to the development of mixed amine systems to capitalize on the strengths of each class. Studies have also delved into the modification of amine structures through the introduction of sterically hindered amines, polyamines, or amine-functionalized materials that can reduce regeneration energy while maintaining high CO₂ absorption capacity [11]. Despite these advancements, the process of optimizing amine-based solvents remains labor-intensive, relying heavily on experimental trial and error.

To address these challenges, computational methods have emerged as a promising alternative for accelerating the discovery and optimization of new amine solvents. Efforts to identify the optimal amine for CO₂ capture, based on absorption and desorption potential, have predominantly utilized virtual screening from existing databases or enumeration of a limited set of known amines [4, 12, 13]. However, the advent of *de novo* molecular design through generative deep learning has revolutionized the creation of molecules from scratch, enabling the generation of molecules with specific and desired properties. This approach directly learns molecular structures and properties from input data, thereby eliminating the need for predefined rules. Significant advancements in natural language processing (NLP) and machine learning algorithms have been pivotal in this progress. This innovative method has shown remarkable success in exploring vast chemical spaces and designing novel molecules with tailored properties [14–16]. For instance, long-short-term memory (LSTM) networks and genetic algorithms (GA) have been used to generate new molecules, surpassing those in existing databases, as demonstrated by benchmarks like GuacaMol [17]. The scoring-assisted generative exploration (SAGE) method has been developed to design molecules with desired properties [18]. This is achieved by integrating LSTM and GA, using the bridged bicyclic ring and virtual synthesis operators, and incorporating various quantitative structure-activity/property relationship (QSAR/QSPR) models. These generative models facilitate efficient exploration of chemical spaces, leading to the discovery of novel molecules.

In this study, the SAGE framework was extended to specifically target the development of new amine solvents for CO₂ capture, referred to as SAGE-Amine. This approach integrates advanced generative modeling methods with QSPR models to generate and evaluate novel amines for high CO₂ absorption. Initially, the SAGE-Amine models were pre-trained on extensive datasets of various amines. Leveraging autoregressive NLP methods with LSTM, Transformer, vanilla Transformer Decoder (TD), and modified Transformer Decoder (X-Transformer Decoder, XTD), the quality of molecules generated by the pre-trained models were compared. Secondly, benchmarking with the pre-trained models was performed to identify known amines for CO₂ capture and to generate new amines with specific molecular formulas. Thirdly, SAGE-Amine’s capabilities were assessed through single-property optimization (SPO) tasks, focusing on achieving high pKa, low viscosity, and low vapor pressure separately in primary and secondary amines, tertiary, cyclic and polyamines, and even irrespective of amine types. Additionally, multiple-property optimization (MPO) tasks were conducted to target high CO₂ absorption along with high pKa, low viscosity, low vapor pressure, high water solubility, high synthetic accessibility, low cost, and moderate boiling and melting points. Lastly, quantum-chemical simulations using COSMO-RS were performed, confirming the potential of the generated amines. The results demonstrated that SAGE-Amine could effectively navigate the chemical space of amines and optimize multiple properties simultaneously, making it a powerful tool for early-stage material discovery.

2 Methods

2.1 Scoring-Assisted Generative Exploration for Amines (SAGE-Amine)

Scoring-assisted generative exploration (SAGE) utilizes an iterative fine-tuning approach to create new molecules [18, 19]. This is achieved through autoregressive NLP and chemical diversification operators. The generated molecules are then evaluated using various scoring models to ensure they meet pre-defined objectives, thereby producing high-scoring molecules. The SAGE was extended for Amines (SAGE-Amine) by pre-training LSTM [20, 21], Transformer [22], vanilla Transformer Decoder (TD) [23], and modified Transformer Decoder (X-Transformer Decoder, XTD) [24–38] models. Furthermore, amine-specific QSPR scoring models were integrated into SAGE-Amine.

The amines utilized in SAGE-Amine are encoded as character sequences in the Simplified Molecular Input Line Entry System (SMILES) format [39]. The amine structures used for pre-training the SAGE-Amine models were sourced from various QSPR datasets [40–44] and in-stock ZINC20 [45], as summarized in Table 1. The amines were categorized into

Table 1: Summary of Datasets used in this work

Class	Task	Unit	All set
Pre-train	Amine-250	Count	706,279
	Amine250-reduced		701,114
	Amine300		2,133,461
	Amine300-reduced		2,127,298
QSPR	Viscosity	$\log_{10}(\text{cP})$	3582
	Vapor Pressure	$\log_{10}(\text{mmHg})$	2945
	Boiling Point	$^{\circ}\text{C}$	23,044
	Melting Point	$^{\circ}\text{C}$	9721

two groups by molecular weight: those with a weight of 250 or less (Amine250) and those with a weight of 300 or less (Amine300). To avoid similarity with target amines used in goal-directed benchmarks, amines with a maximum similarity exceeding 0.323 were excluded, as calculated by the Morgan fingerprint in RDKit [46]. This exclusion resulted in reduced datasets (Amine250-reduced and Amine300-reduced). These four datasets were then randomly split into training and validation sets, with proportions of 0.998 and 0.002, respectively.

The NLP components in SAGE-Amine for autoregressive generation include LSTM, Transformer, TD, and XTD models. The LSTM model comprises three layers with 1,024 hidden units, a dropout probability of 0.2, a learning rate of 0.001, and a batch size of 512. The Transformer model was trained with eight attention heads, three encoder and decoder layers, 1,024 hidden units, a dropout probability of 0.2, an embedding size of 256, a learning rate of 0.001, and a batch size of 512. The TD and XTD models were trained similarly but utilized only the decoder layers.

The XTD incorporates several modifications to the TD model [24–38]. Firstly, it includes 20 learned memory tokens that are processed through the attention layers alongside the input tokens to alleviate outliers [25]. Secondly, it employs layer normalization through L2-normalized embeddings to improve convergence [26]. Within the attention layer, it integrates rotary embeddings and T5 simplified embeddings with relative positional embeddings [27, 28]. It shifts a subset of the feature dimension along the sequence dimension by one token to aid convergence [30]. Furthermore, the XTD gates the residual connections within the transformer network to enhance stability and performance [31]. It utilizes a single head for keys and values but maintains multi-headed queries for memory efficiency [33]. The queries and keys are L2-normalized along the head dimension before the dot product (cosine similarity) to prevent the attention operation from overflowing [34]. An efficient method is used to sparsify attention by zeroing all dot-product query/key values that do not fall within the top k values [35]. Information is mixed between heads both before and after attention (softmax) [36]. The normformer is applied to provide per-head scaling after aggregating the values in attention, which aids convergence, and an extra layer normalization is applied right after the activation in the feedforward process for performance improvement [32]. Gated linear unit variants are included for performance enhancements [37], and there is no bias in the feedforward layers to increase throughput without any loss of accuracy [38].

The NLP models were pre-trained with the Adam optimizer [47] over 150 epochs across four datasets. The final model weights were selected based on achieving the lowest loss on the validation sets. The generated amines were assessed using several performance metrics: validity, uniqueness, novelty, diversity, and the ratios of amines and amine types (primary, secondary, tertiary, cyclic, and polyamines). Validity evaluates the model’s capability to integrate chemically accurate constraints and syntax in SMILES, ensuring correct valence. Uniqueness measures the model’s ability to produce a varied set of amines, avoiding a limited range. Novelty is gauged by the percentage of generated amines absent from the training data. Diversity is evaluated by analyzing the chemical variation within the generated molecule sets, determined using sphere exclusion diversity (SEDiv [48]). The ratios of amines refer to the proportion of molecules containing an amine group within the generated set. The ratio of amine types reflects the distribution of these amines into their respective categories based on the number of hydrogen atoms attached to the nitrogen atom. Notably, even in cases of polyamines, the presence of an amine within a ring structure classifies it as cyclic.

The pre-trained NLP models in SAGE-Amine generate amines autoregressively in each iteration, first verifying the generated amines to ensure they have valid SMILES strings and do not contain radicals. Next, the molecules are checked to confirm if they are amines and, if so, to determine their specific amine type. Following the SAGE framework [18], chemical diversification operators, including mutation and crossover, are then applied. The mutation operator introduces various chemical modifications at the atomic level, such as appending atoms, inserting atoms, altering bond orders in covalent bonds, adding or removing ring bonds, and creating bridged bicyclic rings in a ring substructure. The crossover

operator randomly splits a pair of parent molecules into fragments and recombines them to form a new molecule at the functional group level, even allowing attachment to bridgehead atoms in bridged bicyclic rings.

After chemical diversification, the molecules are re-evaluated to confirm their status as amines. These amines are then assessed according to predefined objectives, are ranked based on their scores, and the top 1,024 amines are stored in a buffer. This buffer is used to fine-tune the NLP model with a learning rate of 0.001 and a batch size of 256 for 8 epochs. The GA and NLP-only models (LSTM, TD, and XTD) each generate 16,384 molecules. In the LSTM/GA, TD/GA, and XTD/GA models, the NLP model generates 8,192 molecules while the GA produces an additional 8,192. The GA-only models initially select 16,384 amines randomly from the training data and generate 16,384 molecules. In all tasks, SAGE-Amine generates molecules over 100 iterations.

2.2 Goal-Directed Benchmarks and Score Definition in SAGE-Amine

Goal-directed benchmarks for evaluating the performance of generative models were established following the protocols used in the GuacaMol [17] and SAGE [18] studies. Rediscovery tasks involved identifying specific target amines, namely 2-aminoethanol (MEA), 2-amino-2-hydroxymethyl-1,3-propanediol (AHMPD), diethanolamine (DEA), diethylamine (DA), N,N-diethylethanolamine (DEEA), N-methyldiethanolamine (MDEA), 2-methylpiperazine (2-MPZ), 2-piperidineethanol (2-PPE), homopiperazine (HomoPZ), and diethylenetriamine (DETA). Similarity tasks required generating amines similar to a target amine, selecting the top 100 generated amines with a similarity score above 0.7, and using their average similarity for evaluation. The amines used for similarity tasks included 2-amino-2-methyl-1-propanol (AMP), isopropylamine (IPA), 3-(isopropylamino)propanol (IPAP), 4-dimethylamino-1-butanol (4DMA1B), 1-dimethylamino-2-propanol (1DMA2P), 1-methyl-piperazine (1-MPZ), 1-ethyl-piperazine (EPZ), piperazine (PZ), 1-(2-aminoethyl)piperazine (AEP), and Triethylenetetramine (TETA). Median similarity tasks used the average similarity value for two target amines, again selecting the top 100 with a similarity score above 0.7. The amines used for these tasks were 2-(2-diethylaminoethoxy)ethanol (DEAE-EO), 1-methyl-2-piperidinemethanol (1M-2PPE), and 1-(2-hydroxyethyl)piperidine (1-(2HE)PP). Isomer tasks involved generating ions that matched a specified molecular formula, addressing the issue of overfitting by ensuring the production of diverse ions rather than those following a simple pattern. The molecular formulas of $C_4H_{11}NO$ originated from AMP, $C_4H_{11}NO_2$ from IPAP, DEEA, and 4DMA1B, and $C_5H_{12}N_2$ from 1-MPZ, 2-MPZ, and HOMO PZ. For all goal-directed benchmarks, similarity scores were computed using the Extended-connectivity fingerprints (ECFP6) [49].

Single-property optimization (SPO) tasks involve the maximization of basic pKa and the minimization of viscosity or vapor pressure in amines by generating amines using SAGE-Amine. Additionally, to perform SPO tasks based on amine type, three separate generations were conducted: one for primary and secondary amines, one for tertiary, cyclic, and polyamines, and one without constraints. For cases where the generated amine did not match the desired type, a penalty was applied by reflecting only 10% of the score. The pKa values of all titratable sites were predicted within the molecule through MolGpKa [40], where the average pKa value of the amine groups was used as the score. Viscosity and vapor pressure were predicted at a standard temperature of 298.15 K.

Multiple-property optimization (MPO) tasks were designed to maximize the CO_2 absorption of amines. To achieve this, a range of factors were considered including basicity (pKa), viscosity, vapor pressure, boiling point, melting point, aqueous solubility, synthetic accessibility, and chemical price. Similar to the SPO tasks, penalties were applied based on the type of amine, used average scores for pKa, and predicted viscosity and vapor pressure at 298.15 K. Next, several adjustments were performed to create weights for these various properties, determining maximum and minimum limits and evaluating them linearly within these ranges. For pKa, a value greater than 14 resulted in a score of 1, while a value less than 7 resulted in a score of 0. For viscosity, a value greater than 2 resulted in a score of 0, while a value less than -1 resulted in a score of 1. For vapor pressure, values above 3 scored 0, and values below -3 scored 1. For boiling point, values below 80 scored 0, and values above 250 scored 1. For melting point, values above 80 scored 0, and values below 40 scored 1. Aqueous solubility (\log_{10} mol/L) was predicted using SolTranNet [50]; predicted values (LogS, mol/L) below -4 scored 0, and values above 2 scored 1. To determine synthetic accessibility, the retrosynthetic accessibility score (RAscore) was employed [51], a metric that rapidly estimates a molecule’s synthetic feasibility. A score closer to 1 indicates a higher probability of finding feasible retrosynthetic pathways, reflecting the molecule’s ease of synthesis. The chemical price was predicted through CoPriNet [52]; predicted values (\$/gram) below 0 were assigned a score of 1, while those above 10 received a score of 0. The MPO score was calculated as the average of these eight scores (pKa, viscosity, vapor pressure, boiling point, melting point, aqueous solubility, synthetic accessibility, and price), along with the target CO_2 absorption score.

2.3 Quantitative Structure-Property Relationship (QSPR)

The datasets for viscosity ($\log_{10}\text{cP}$), vapor pressure ($\log_{10}\text{mmHg}$), boiling point ($^{\circ}\text{C}$), and melting point ($^{\circ}\text{C}$) are summarized in Table 1. The viscosity data were sourced from Chew *et al.* [41], while the vapor pressure, boiling point, and melting point data were obtained from EPI Suite 4.11 [43]. Additionally, some boiling point data were manually supplemented from other sources [42, 44, 53]. The maximum and minimum values for each dataset are as follows: viscosity ranges from -1 to 1.4236, with a temperature spanning 227.45 to 404.10 K. Vapor pressure ranges from -20.7399 to 7, with a temperature spanning 205.15 to 448.15 K. Boiling point values range from -268.935 to 5900 $^{\circ}\text{C}$, and melting point values range from -219.61 to 3410 $^{\circ}\text{C}$.

Molecular fingerprints were employed to generate numerical features of chemicals. Based on PyFingerprint [54], the 11 types of molecular fingerprints were created: Avalon, ECFP6, Extended, FCFP4, MACCS, Morgan, PCFP, rDesc, rPair, rTorsion, and Standard. The Avalon fingerprint utilizes a generator that enumerates specific paths and feature classes of the molecular graph [55]. Extended-connectivity fingerprints with a diameter of 6 (ECFP6) are designed for structure-activity relationship modeling, representing circular atom neighborhoods as 1024-bit keys [49]. The Extended fingerprint is a 1024-bit hashed fingerprint that considers rings and atomic properties. Function-class fingerprints with a diameter of 4 (FCFP4) are similar to ECFP and index pharmacophore-like roles of distinct atoms within molecules as 1024-bit keys. The Molecular Access System (MACCS) is a widely used fingerprint for assessing structural similarity using 166-bit MACCS keys [56], while the PubChem system employs substructural fingerprints (PCFP) with 881-bit structural keys to represent chemical structures, facilitating similarity and neighbor searches [53]. The rDesc, rPair, and rTorsion descriptors are derived from RDKit [46] and include rd-descriptor, topological torsion, and atom-pair [57]. The Standard fingerprint is a 1024-bit hashed fingerprint that considers paths of a given length. Additionally, six fingerprints were concatenated with MACCS fingerprints: Avalon, ECFP6, Extended, FCFP4, PCFP, and Standard to create a comprehensive fingerprint set.

To develop QSPR models using these fingerprints, several regression algorithms were applied: Random Forest (RF), Light Gradient Boosting Machine (LGBM), and Extreme Gradient Boosting (XGB). These algorithms utilize decision trees to minimize overfitting and reduce variance. Each decision tree evaluates numerical features to produce continuous outputs, constructed sequentially and refined based on previous errors. To identify the most effective QSPR models, a grid search was conducted, considering three hyperparameters for LGBM, two for RF, four for XGB, and two for GB. Detailed hyperparameter tuning for the QSPR models is provided in Table S2. For LGBM, the hyperparameters were booster type (boosting_type), the number of gradient-boosted trees (n_estimators), and the learning rate (learning_rate) [58]. Those of RF were the number of trees (n_estimators) and the maximum tree depth (max_depth) [59]. Those of XGB included booster type (booster), the number of trees (n_estimators), maximum tree depth (max_depth), and learning rate (learning_rate) [60]. A fixed random seed was used to perform a stratified split for 5-fold cross-validation, ensuring a balanced distribution by dividing the y-values into quintiles.

Additionally, a molecular graph was utilized through the application of a directed message-passing neural network (D-MPNN) to develop QSPR models. The molecular graph captures detailed atomic features such as atom symbol, degree, valence, formal charge, chirality, radical presence, hybridization, the number of hydrogen atoms, and aromaticity. It also captures bond characteristics including bond type, conjugation, ring presence, and stereo configuration. Atom nodes are represented by several one-hot encoded vectors capturing chemical characteristics: atom symbols (44-dimensional), degree (12-dimensional), valence (8-dimensional), formal charge (1-dimensional), chirality (5-dimensional), radical presence (1-dimensional), hybridization (6-dimensional), the number of hydrogen atoms (6-dimensional), and aromaticity (1-dimensional). Bond edges are similarly represented by vectors indicating bond type (5-dimensional for single, double, triple, aromatic, and unknown), conjugation (1-dimensional), ring presence (1-dimensional), and stereo configuration (7-dimensional). The D-MPNN updates node attributes by aggregating information from neighboring nodes; however, D-MPNN treats edges as directed [61]. It outputs the target property from the embedding for a molecule’s sub-structure, highlighting essential features such as atom symbol, connectivity, and bond type. The hyperparameters for D-MPNN are the hidden units for the embedding (hidden_unit) and the number of message-passing and updating rounds (steps).

2.4 Conductor-like Screening Model for Real Solvents (COSMO-RS)

The Conductor-like Screening Model for Real Solvents (COSMO-RS) is a quantum chemistry-based statistical thermodynamics model that enables the prediction of thermodynamic properties of fluids and liquid mixtures [62]. In COSMO-RS, the free energy of each species in solution is determined by calculating its chemical potential through a statistical thermodynamics algorithm, which iteratively evaluates system affinity to molecular surface polarity [63, 64]. Amines used in the goal-directed benchmark sets and the top-performing amines generated through SAGE-Amine were selected using COSMOtherm (COSMOlogic GmbH, Leverkusen, Germany). The structures of the amines were prepared using LigPrep in the Schrödinger suite [65], and single conformers with the lowest ground-state energy were

chosen for each amine. COSMO-RS calculations at the BP-TZVPD-FINE level were subsequently performed using TURBOMOLE [66]. These calculations involved full geometry optimization using density functional theory (DFT) with the Becke–Perdew (BP86) functional [67, 68] and DFT-D3 dispersion correction [69], employing a grid size of m3 and the resolution of identity (RI) approximation [70]. The triple- ζ valence polarized (def-TZVP) basis set was used for the optimization, followed by single-point energy calculations with the same DFT/BP86-D3/RI method incorporating diffuse functions via the def2-TZVPD basis set. Thermodynamic analyses were conducted to determine CO₂ Henry’s law constant (MPa), CO₂ solubility ($\log_{10} X_{\text{sol}}$), flash point (°C), vaporization enthalpy (kJ/mol), excess enthalpy (kJ/mol), and excess Gibbs free energy (kJ/mol) for a water-amine mixture (80wt% water, 20wt% amine) as well as the flash point of the pure amine. All calculations were performed at 323.15 K using the COSMOtherm modules.

3 Results

3.1 Scoring-Assisted Generative Exploration for Amine (SAGE-Amine)

Unlike traditional virtual screening, which identifies the best chemicals from known existing databases, generative models aim to design molecules from scratch that possess desired properties. Scoring-Assisted Generative Exploration (SAGE) alternates between generation and evaluation phases to discover new chemicals [18, 19]. During generation, molecules are created through autoregressive modeling and chemical diversification, while the evaluation phase iteratively refines the NLP model using multiple scoring metrics to optimize the generated compounds.

For amine design in CO₂ absorption, this framework was extended into SAGE-Amine (Figure 1), which operates with a generation and evaluation phase. The generation phase uses NLP models such as LSTM, Transformer, TD, and XTD, pre-trained on amine-specific datasets. These models generate token sequences autoregressively, creating new chemicals similar to compounds in pre-training datasets. Similar to the original SAGE, the generated molecules undergo further modifications via chemical diversification, broadening the chemical space.

In the evaluation phase, the generated molecules are validated to ensure they represent real chemicals by confirming valid SMILES, non-radically, and the presence of amine groups. Various properties relevant to efficient CO₂ absorption, such as basicity (pKa), viscosity, vapor pressure, boiling and melting points, aqueous solubility, synthetic accessibility, and cost, are predicted using QSPR models. The generated amines are ranked, and the top-ranked amines are selected to fine-tune the NLP models, enabling scoring-assisted generative exploration. This process facilitates both single-property optimization (SPO) and multiple-property optimization (MPO) tasks.

3.2 Pre-training the SAGE-Amine with Amine databases

To generate amines, SAGE-Amine required the NLP models, which learned the SMILES format and amine patterns through pre-training. Diverse amine data were gathered from sources like ZINC20 [45] and several QSPR datasets [40–44, 53]. The data was organized into four datasets based on molecular weight thresholds (Amine250, Amine250-reduced, Amine300, and Amine300-reduced), which are summarized in Table 1. Amine250 and Amine300 contained molecules with molecular weights below 250 and 300 g/mol, respectively, while the reduced datasets were created by filtering compounds based on their similarity to target amines in a goal-directed benchmark. The LSTM, Transformer, TD, and XTD algorithms were used to pre-train the models on these datasets.

Once pre-trained, these models generated 5,000 to 10,000 molecules, which were evaluated for validity, uniqueness, novelty, sphere-exclusion diversity, and whether they were amines (Table S1). When trained on the Amine250 and Amine250-reduced datasets, all four models generated over 90% valid molecules. The LSTM and TD models showed high uniqueness, both producing over 95% unique molecules, while Transformer and XTD had lower uniqueness rates of 61% and 77%, respectively. For novelty, the TD and XTD generated many new molecules not found in the training set, while the LSTM and Transformer produced more familiar compounds. The diversity of the generated molecules also varied. LSTM and TD excelled in diversity, while Transformer and XTD produced less diverse molecules. In terms of generating amines, LSTM, Transformer, and TD generated over 95% amines, while the XTD generated about 80%. Only the XTD effectively generated both cyclic and more complex amines, while the other models mainly produced cyclic amines. When using the Amine300 and Amine300-reduced datasets, the models performed similarly, generating over 90% valid SMILES, although the XTD on Amine300-reduced had a lower validity rate of 50%. The patterns of uniqueness, novelty, and diversity remained consistent, with LSTM, TD, and XTD generating diverse molecules.

From an algorithmic perspective, all models demonstrated the capability to generate valid amines, with distinct differences in novelty and diversity. The LSTM primarily produced cyclic amines from the training set, showing relatively low novelty. In contrast, the TD generated more novel molecules while still favoring cyclic amines. The XTD excelled, producing a diverse mix of cyclic and polyamines, along with high novelty. However, the Transformer

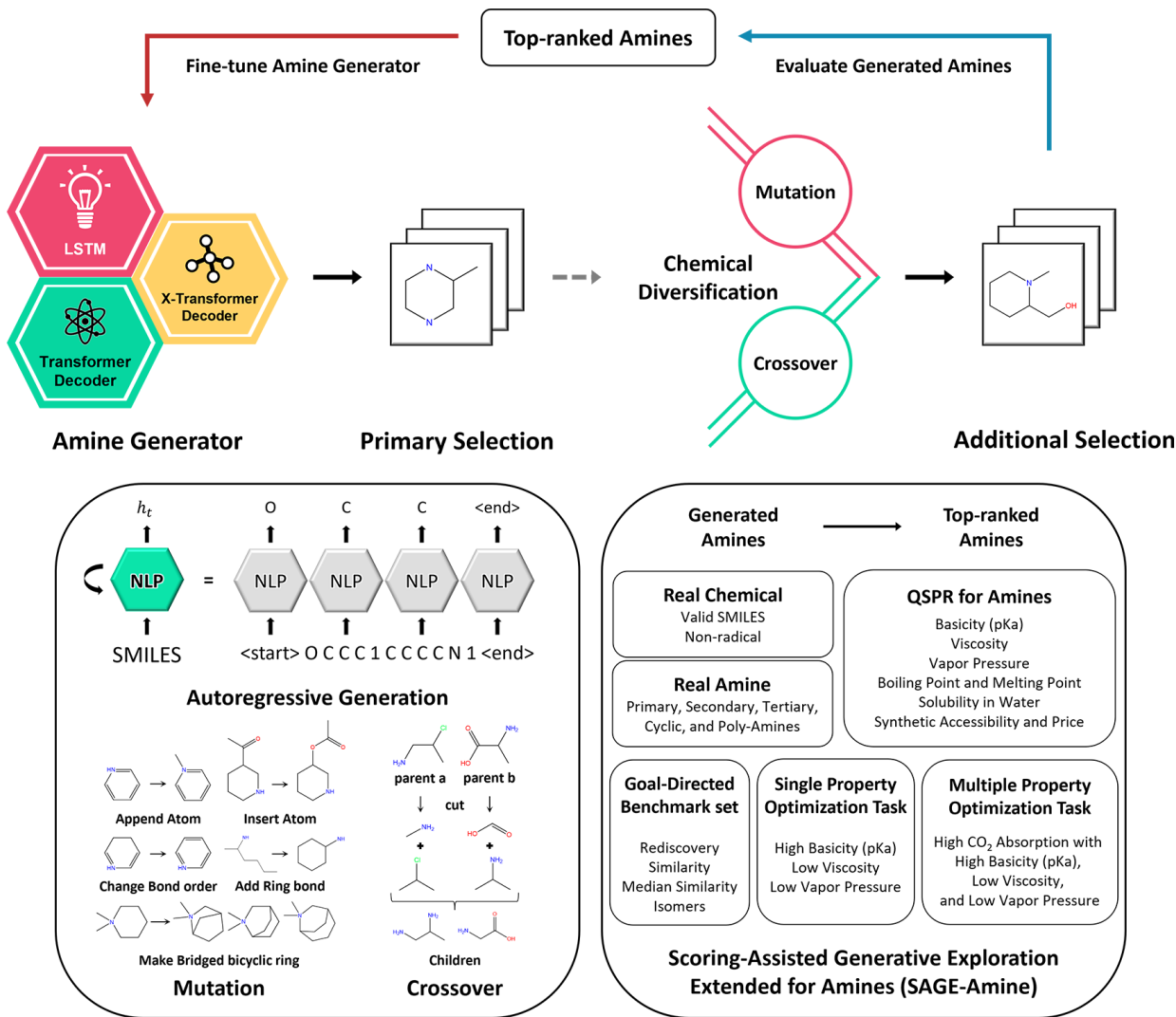


Figure 1: Scoring-Assisted Generative Exploration Extended for Amines (SAGE-Amine)

model had low novelty, generating mainly known amines from the training set. From a dataset perspective, pre-training with the Amine300 dataset yielded better results compared to Amine250, with improved validity, uniqueness, and diversity. Among the reduced datasets, Amine250-reduced outperformed Amine300-reduced, offering a better balance between dataset size and optimization efficiency. Overall, the LSTM, TD, and XTD were identified as the most effective algorithms, with the Amine250-reduced and Amine300 datasets proving most suitable for pre-training. These results indicate that the combination of algorithm and dataset selection plays a critical role in generating novel, diverse amines optimized for CO₂ capture.

3.3 Goal-directed Benchmarks for SAGE-Amine Evaluation

In the previous phase, the NLP models generated molecules without specific objectives, focusing on validating their status as real amines and analyzing the types produced. To push this further, goal-directed benchmarks were prepared to evaluate how well the models could generate amines that meet specific targets, as outlined in Table 2. This shift from unguided generation to targeted design allows for a more precise assessment of the model’s ability to create compounds tailored to particular criteria.

These benchmarks focused on four key tasks: rediscovery, similarity, median similarity, and isomer generation. Specifically, they aimed to evaluate how well the models could rediscover known amines, generate structurally similar molecules, create isomers with defined molecular formulas, and design amines that fall between two target structures.

Table 2: Results of the SAGE-Amine Models for the Goal-Directed Benchmarks

Task	Name	Amine Type	GA	LSTM	LSTM/GA	TD	TD/GA	XTD	XTD/GA
Rediscovery	MEA	Primary	0.444	1.000	1.000	1.000	1.000	1.000	1.000
	AHMPD	Primary	0.441	1.000	1.000	1.000	1.000	1.000	1.000
	DEA	Secondary	0.600	1.000	1.000	1.000	1.000	1.000	1.000
	DA	Secondary	0.522	1.000	1.000	1.000	1.000	1.000	1.000
	DEEA	Tertiary	1.000	1.000	1.000	1.000	1.000	1.000	1.000
	MDEA	Tertiary	1.000	1.000	1.000	1.000	1.000	1.000	1.000
	2-MPZ	Cyclic	1.000	1.000	1.000	1.000	1.000	1.000	1.000
	2-PPE	Cyclic	1.000	1.000	1.000	1.000	1.000	1.000	1.000
	HomoPZ	Cyclic	0.567	1.000	1.000	1.000	1.000	1.000	1.000
	DETA	Poly	0.600	1.000	1.000	1.000	1.000	1.000	1.000
Similarity	AMP	Primary	0.777	0.817	0.817	0.817	0.817	0.815	0.817
	IPA	Primary	0.617	0.790	0.790	0.790	0.790	1.000	0.790
	IPAP	Secondary	0.796	0.842	0.842	0.842	0.842	0.837	0.842
	4DMA1B	Tertiary	0.814	0.851	0.851	0.851	0.851	0.731	0.851
	1DMA2P	Tertiary	0.768	0.828	0.828	0.828	0.828	0.831	0.828
	1-MPZ	Cyclic	0.672	0.812	0.812	0.807	0.807	0.806	0.808
	EPZ	Cyclic	0.634	0.896	0.896	0.895	0.894	0.896	0.895
	PZ	Cyclic	0.377	0.766	0.766	0.766	0.764	0.766	0.776
	AEP	Cyclic	0.687	0.906	0.906	0.904	0.904	0.863	0.911
	TETA	Poly	0.739	0.930	0.930	0.930	0.939	0.943	1.000
Median Similarity	DEAE-EO and 1M-2PPE		0.277	0.395	0.395	0.395	0.395	0.313	0.395
	DEAE-EO and 1-(2HE)PP		0.335	0.398	0.398	0.398	0.398	0.364	0.395
	1M-2PPE and 1-(2HE)PP		0.428	0.462	0.462	0.438	0.441	0.431	0.437
Isomers	C ₄ H ₁₁ NO		0.997	1.000	1.000	1.000	1.000	1.000	1.000
	C ₄ H ₁₁ NO ₂		0.903	1.000	1.000	1.000	1.000	1.000	1.000
	C ₅ H ₁₂ N ₂		0.907	0.999	1.000	1.000	1.000	1.000	1.000
	C ₆ H ₁₅ NO		0.920	1.000	1.000	1.000	1.000	1.000	1.000
Total			18.821	23.692	23.693	23.660	23.671	23.596	23.744

For an evaluation, three approaches were employed: (1) using a genetic algorithm (GA) for chemical diversification, (2) using pre-trained NLP models (LSTM, TD, and XTD), and (3) combining the NLP models with GA to form hybrid models (LSTM/GA, TD/GA, and XTD/GA). Each of the seven models generated an equal number of molecules, which were validated as real chemicals and amines before scoring based on their performance in the benchmarks.

The target molecules were 23 amines known for their efficiency in CO_2 capture. The tasks included rediscovering these specific amines, creating structurally similar ones, generating isomers with defined molecular formulas, and producing amines that bridged two target molecules in terms of structure. In the rediscovery task, all models except GA performed perfectly, with GA scoring 7.174. In the similarity task, the XTD/GA model achieved the highest score (8.518), followed by XTD and LSTM/GA. For the median similarity task, LSTM/GA and LSTM achieved the best scores, while GA lagged. In the isomer generation task, all models except LSTM and GA scored the maximum of 4.000, with GA scoring the lowest. Overall, the XTD/GA model demonstrated the best performance across all benchmarks, achieving a total score of 23.744, followed by LSTM/GA and LSTM. This indicates that combining NLP models with GA yields better results in tasks requiring structural diversification and optimization. The goal-directed benchmarks highlight the strengths of each approach, particularly in challenging tasks such as amine rediscovery and isomer generation.

3.4 Single Property Optimization with SAGE-Amine

Based on the goal-directed benchmark results, the combination of NLP and GA approaches outperformed using NLP alone, making LSTM/GA, TD/GA, and XTD/GA in SAGE-Amine particularly effective for de novo amine design. In generating amines optimized for CO₂ capture using SAGE-Amine, several key factors must be considered, including high cyclic capacity, rapid absorption rate, low enthalpy of absorption, and high equilibrium temperature sensitivity [71]. Firstly, an effective amine should demonstrate high cyclic capacity, which includes both high absorption capacity and efficient desorption of CO₂. The dissociation constant (pKa) is generally correlated with CO₂ absorption and cyclic capacity, with tertiary amines showing a strong correlation, while primary and secondary amines tend to exhibit less correlation [4]. Secondly, the amine should react rapidly with CO₂. Higher pKa values are typically associated with faster reaction rates [71]. Thirdly, the amine should have low regeneration energy requirements. A lower heat of absorption is preferred to minimize the energy required for desorption. Additionally, low viscosity is beneficial in reducing energy consumption during processing. Finally, the vapor pressure of the amine should be low to minimize volatility, reducing solvent loss through evaporation, which in turn enhances cost-effectiveness.

Single property optimization (SPO) tasks were focused on optimizing three essential properties for efficient CO₂ absorption: basicity (pKa), viscosity, and vapor pressure. For predicting pKa, the MolGpKa model was employed, which achieved an RMSE of 0.47, an MAE of 0.29, and an R² of 0.97 [40], demonstrating high accuracy in predicting the basicity of amines. In contrast, the datasets for viscosity and vapor pressure were collected and are summarized in Table 1. Our QSPR models for these properties were specifically developed by combining molecular fingerprints with gradient boosting models, as well as molecular graphs with D-MPNN. To identify the optimal hyperparameters, a grid search was conducted with 5-fold cross-validation, with the explored hyperparameters summarized in Table S2. The performance metrics for the best models, selected based on the product of the R² scores from the training and cross-validation sets, are detailed in Tables S3- S5, with the metrics of the final models presented in Table S6. As a result, the QSPR model for predicting viscosity, using rDesc/LGBM, achieved an R² of 0.9605 and an MAE of 0.0468 on the test set. Similarly, the vapor pressure model, using Graph/D-MPNN, performed with an R² of 0.9952 and an MAE of 0.2016 on the test set.

These three QSPR models were integrated into SAGE-Amine to create three SPO tasks aimed at either increasing pKa, reducing viscosity, or lowering the vapor pressure of amines. Additionally, three different types of restrictions on the amine generation process were applied: generating only primary and secondary amines, generating only tertiary, cyclic, and polyamines, and generating amines without any restrictions. Using three different models (LSTM/GA, TD/GA, and XTD/GA), amines were generated over 100 steps for each SPO task. The results of these SPO tasks are summarized in Table 3.

The SPO tasks for generating amines with high pKa values were carried out using three different models, with three amine-type restrictions. The results are illustrated in Figure S1. First, the models were used to primarily generate primary and secondary amines, as shown in Figure S1A. The LSTM/GA model achieved a median pKa value of 10 by the 3rd step, and values of 12 and 14 by the 7th and 12th steps, respectively. The TD/GA model generated amines with median pKa values above 10, 12, and 14 at the 3rd, 9th, and 30th steps. The XTD model surpassed pKa values of 10 and 12 at the 10th and 27th steps but did not exceed a median pKa of 14. Based on maximum values, the LSTM/GA, TD/GA, and XTD/GA models predicted amines with pKa values of 17.338, 15.177, and 14.034, respectively.

Similarly, the models were tasked with generating tertiary, cyclic, and polyamines, which are shown in Figure S1B. The LSTM/GA model produced amines with median pKa values above 10, 12, and 14 at the 3rd, 7th, and 8th steps. The TD/GA achieved this at the 3rd, 7th, and 34th steps, while the XTD model did so at the 3rd, 21st, and 21st steps. For maximum values, the LSTM/GA, TD/GA, and XTD/GA models generated amines with predicted pKa values of 20.344, 19.453, and 16.137, respectively. Finally, when no restrictions were applied to the type of amine generated, the LSTM/GA model produced amines with median pKa values above 10, 12, and 14 at the 2nd, 8th, and 12th steps. The TD/GA exceeded 10 and 12 at the 3rd and 7th steps but did not surpass 14. The XTD model exceeded pKa values of 10, 12, and 14 at the 3rd, 18th, and 25th steps. In terms of maximum values, the LSTM/GA, TD/GA, and XTD/GA models generated amines with predicted pKa values of 16.475, 14.241, and 15.599, respectively. In summary, all three models were able to generate amines with predicted pKa values above 14, confirming that SAGE-Amine is effective at producing amines with high pKa values.

Similarly, the SPO task was performed to reduce viscosity, and the results are shown in Figure S2. First, the models were used to primarily generate primary and secondary amines with lower viscosity, as illustrated in Figure S2A. The LSTM/GA model produced amines with a viscosity below 0.5 by the 4th step, and values of 0 and -0.5 at the 6th and 47th steps. The TD/GA model reached these values at the 4th, 6th, and 63rd steps, while the XTD/GA model achieved 0.5 and 0 viscosity at the 6th and 10th steps but did not reach -0.5. Looking at the minimum values, the models generated amines predicted to have viscosities of -0.753, -0.764, and -0.668, respectively.

Table 3: Results of the SAGE-Amine Models for the Property Optimization Tasks

Task	Objective	Amine Type	LSTM/GA	TD/GA	XTD/GA
Single Property Optimization	High pKa	Primary and Secondary	17.338	15.177	14.034
		Tertiary, Cyclic, and Poly	20.344	19.453	16.137
		No restriction	16.475	14.241	15.599
	Low Viscosity	Primary and Secondary	-0.753	-0.764	-0.668
		Tertiary, Cyclic, and Poly	-0.838	-0.832	-0.830
		No restriction	-0.838	-0.841	-0.844
	Low Vapor Pressure	Primary and Secondary	-25.774	-25.898	-24.001
		Tertiary, Cyclic, and Poly	-25.750	-26.151	-25.877
		No restriction	-25.922	-26.151	-25.878
Multiple Property Optimization	High CO ₂ Absorption	Primary and Secondary	0.870	0.873	0.921
		Tertiary, Cyclic, and Poly	0.858	0.909	0.878
		No restriction	0.863	0.868	0.914

Next, the task was to generate tertiary, cyclic, and polyamines, as shown in Figure S2B. The LSTM/GA model achieved viscosities of 0.5, 0, and -0.5 at the 3rd, 5th, and 17th steps, while the TD/GA achieved this at the 3rd, 6th, and 19th steps, and the XTD/GA at the 3rd, 7th, and 50th steps. For minimum values, the LSTM/GA, TD/GA, and XTD/GA models produced amines with viscosities of -0.838, -0.832, and -0.830, respectively. Finally, when no restrictions were applied to the type of amine generated, the results are shown in Figure S2C. The LSTM/GA model generated amines with viscosities below 0.5, 0, and -0.5 by the 3rd, 5th, and 19th steps. The TD/GA achieved this at the 3rd, 6th, and 19th steps, and the XTD at the 2nd, 5th, and 17th steps. In terms of minimum values during the 100-step SPO task, the LSTM/GA, TD/GA, and XTD/GA models generated amines with predicted viscosities of -0.838, -0.841, and -0.844, respectively. In conclusion, all three models effectively generated amines with viscosities lower than -0.5, demonstrating that SAGE-Amine can successfully design amines with reduced viscosity.

Lastly, SPO tasks were performed to reduce the vapor pressure of amines, and the results are shown in Figure S3. First, the models were used to generate primary and secondary amines with lower vapor pressure, as seen in Figure S3A. The LSTM/GA model produced amines with predicted vapor pressure values of -5, -10, and -20 at the 1st, 3rd, and 6th steps, based on the median values. The TD/GA model reached these values at the 4th, 6th, and 13th steps, while the XTD/GA model achieved this at the 7th, 9th, and 28th steps. Looking at the minimum values over the 100-step SPO task, the LSTM/GA, TD/GA, and XTD/GA models generated amines with vapor pressures of -25.744, -25.898, and -24.001, respectively.

Next, the task was to generate tertiary, cyclic, and polyamines, as shown in Figure S3B. The LSTM/GA model generated amines with predicted vapor pressures of -5, -10, and -20 at the 1st, 3rd, and 6th steps, based on median values. The TD/GA achieved these values at the 1st, 2nd, and 7th steps, while the X-TD/GA did so at the 1st, 2nd, and 9th steps. Looking at the minimum values, the LSTM/GA, TD/GA, and XTD/GA models created amines with vapor pressures of -25.750, -26.151, and -25.877, respectively. Finally, when generating amines without restrictions on type, the results are shown in Figure S3C. The LSTM/GA model produced amines with predicted vapor pressures of -5, -10, and -20 at the 1st, 3rd, and 5th steps, based on median values. The TD/GA achieved this at the 1st, 2nd, and 7th steps, and the XTD/GA at the 1st, 2nd, and 8th steps. For the minimum values, the LSTM/GA, TD/GA, and XTD/GA models produced amines with vapor pressures of -25.922, -26.151, and -25.878, respectively. In conclusion, all three models successfully generated amines with vapor pressures below -20, demonstrating that SAGE-Amine effectively reduces vapor pressure in amine design.

In summary, the SPO tasks for generating amines with high pKa values, lower viscosity, and reduced vapor pressure demonstrate the effectiveness of SAGE-Amine in producing optimized molecules. Notably, SAGE-Amine’s generative capabilities extend beyond the limits of the experimental database used to develop the QSPR models, pushing into unexplored regions. This extrapolative exploration allowed SAGE-Amine to generate amines predicted to exceed the maximum pKa values and achieve minimum values for viscosity and vapor pressure beyond the boundaries of the original dataset. These results emphasize the strength of SAGE-Amine in discovering novel amines with properties that surpass the constraints of the QSPR training data, offering a powerful tool for amine design in various applications.

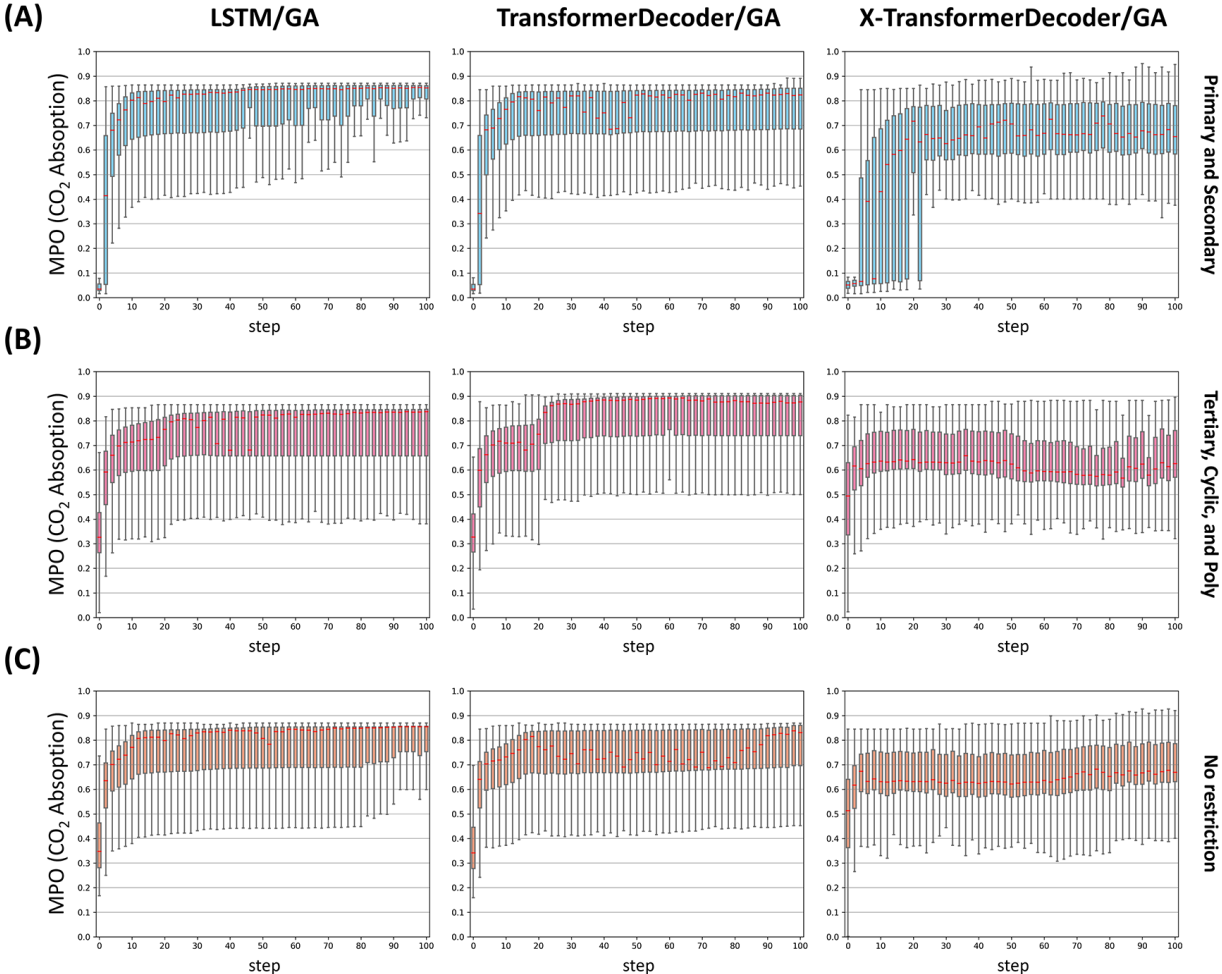


Figure 2: Multiple-Property Optimization Tasks for CO₂ Absorption of Amines. (A) Boxplots illustrate the SAGE-Amine process for optimizing multiple CO₂ absorption properties by generating primary and secondary amines using LSTM/GA, TD/GA, and XTD/GA methods. (B) Boxplots show the generation of tertiary, cyclic, and polyamines for multi-property optimization in CO₂ absorption. (C) Boxplots represent the steps for generating amines without restrictions on amine type. The median in each boxplot is highlighted in red.

3.5 Multiple Property Optimization with SAGE-Amine

Based on the results of the SPO tasks, SAGE-Amine demonstrated its ability to optimize amines by modulating specific single properties and successfully identifying novel candidates with desired characteristics. However, the discovery of novel amines for CO₂ capture demands the simultaneous optimization of multiple properties rather than focusing on a single property. This necessitates the application of multiple-property optimization (MPO). In addition to the properties addressed in the SPO tasks, the CO₂ absorption process must also be economically viable. This requires that the amines be readily synthesizable, cost-effective, water-soluble, and exhibit favorable boiling and melting points that do not impede the cyclic absorption process. To address these requirements, the MPO tasks were prepared to evaluate its potential for discovering amines tailored for CO₂ capture. The evaluation included multiple objectives, including high pKa, low viscosity, low vapor pressure, high synthesizability, affordability, high aqueous solubility, and moderate boiling and melting points. For this purpose, pre-defined criteria were applied, followed by min-max scaling to normalize the objectives. The MPO score was subsequently defined as the average of these scaled objectives, enabling a comprehensive assessment of SAGE-Amine’s performance in meeting the diverse requirements for CO₂ capture applications.

As with the SPO tasks, the MPO tasks for generating amines with multiple desired properties were performed using the LSTM/GA, TD/GA, and XTD/GA models under four amine restriction categories. The results are depicted in Figure 2

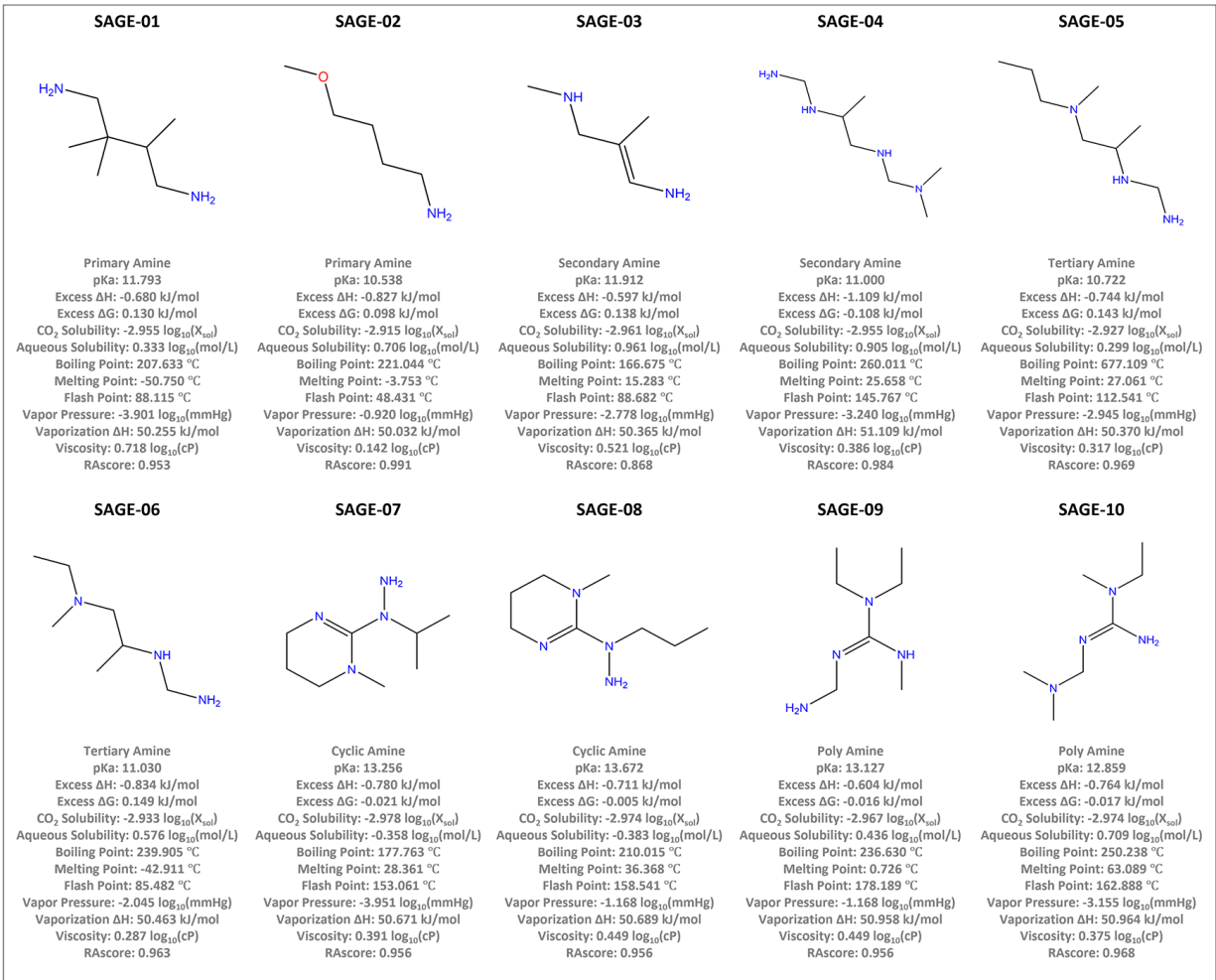


Figure 3: Top-ranked Amines Generated by SAGE-Amine. Top-ranked amines generated by SAGE-Amine and their predicted properties are shown. Carbon, nitrogen, and oxygen atoms are colored black, blue, and red, respectively.

and summarized in Table 3. First, the generation of primary and secondary amines with higher MPO scores was carried out using iterative fine-tuning with SAGE-Amine, as illustrated in Figure 2A. The LSTM/GA model achieved an MPO score exceeding 0.5 by the 3rd step and reached scores of 0.6, 0.7, and 0.8 at the 4th, 6th, and 11th steps, respectively. The TD/GA model attained these scores at the 3rd, 4th, 8th, and 13th steps. In contrast, the XTD/GA model reached scores of 0.5, 0.6, and 0.7 at the 12th, 17th, and 19th steps, respectively, but did not surpass 0.8 at the median level. For maximum MPO scores over the 100-step MPO task, the LSTM/GA, TD/GA, and XTD/GA models generated amines with scores of 0.870, 0.873, and 0.921, respectively.

Next, the task involved generating tertiary, cyclic, and polyamines, as shown in Figure 2B. The LSTM/GA model achieved MPO scores of 0.5, 0.6, 0.7, and 0.8 at the 2nd, 3rd, 8th, and 23rd steps, respectively. The TD/GA model reached these scores at the 2nd, 3rd, 7th, and 22nd steps, while the XTD/GA achieved a score of 0.5 at the 2nd step but did not exceed 0.7 or 0.8 at the median level. In terms of maximum MPO scores, the LSTM/GA, TD/GA, and XTD/GA models achieved values of 0.858, 0.909, and 0.878, respectively. Finally, when no restrictions were applied to the type of amine generated, the results are presented in Figure 2C. The LSTM/GA model produced amines with MPO scores exceeding 0.5, 0.6, 0.7, and 0.8 by the 2nd, 3rd, 5th, and 12th steps, respectively. Similarly, the TD/GA achieved these scores at the 2nd, 3rd, 5th, and 17th steps, whereas the XTD/GA reached scores of 0.5 and 0.6 at the 1st and 2nd steps but failed to exceed 0.7 or 0.8 at the median level. Regarding maximum MPO scores during the 100-step task, the LSTM/GA, TD/GA, and XTD/GA models produced amines with predicted viscosities of 0.863, 0.868, and 0.914, respectively.

To design amines with higher MPO scores for CO₂ capture, the SAGE-Amine models generated 384k primary, 1.21M secondary, 168k tertiary, 869k cyclic, and 2.13M polyamines in nine MPO tasks. The top 300 molecules per class were selected based on MPO scores and their six thermodynamic properties (CO₂ Henry’s law constant, CO₂ solubility, vaporization ΔH , excess ΔH , excess ΔG , and flash point) were predicted via COSMO-RS simulations in a water-amine mixture (80 wt% water and 20 wt% amine). For comparison, the top two amines from each class were analyzed alongside 23 reference amines from the goal-directed benchmark, with predicted properties summarized in Tables S7–S8 and the top 10 illustrated in Figure 3. Compared to the reference median, top-ranked amines showed an increased pKa (+2.853) and boiling point (+86.248), decreased viscosity (-0.237), vapor pressure (-1.529), and melting point (-7.043), while synthetic accessibility, price, and aqueous solubility remaining similar. This indicates that SAGE-Amine effectively guided molecule generation towards the intended objectives. COSMO-RS results further showed a reduced CO₂ Henry’s law constant (-9.222), increased flash point (+9.903), slightly lower vaporization ΔH (-0.280), and comparable CO₂ solubility, excess ΔH , and excess ΔG . Overall, the SAGE-Amine generated top-ranked amines competitive with references while achieving target objectives, highlighting the potential of generative models for task-specific amine discovery in CO₂ capture.

4 Discussion

The de novo design of molecules using generative models is emerging as a viable alternative to traditional methods such as virtual screening and combinatorial enumeration. In this study, the SAGE framework was extended to develop SAGE-Amine, tailored for amine generation in CO₂ absorption applications. By leveraging SMILES-based NLP models pre-trained on diverse amine structures, the SAGE-Amine enabled the autoregressive generation of novel amines with high validity, uniqueness, and diversity. Our findings suggest that different NLP architectures exhibit varying generative tendencies: LSTM and Transformer models primarily reproduced training set molecules, while TD and XTD generated a higher proportion of novel amines. Incorporating GA further enhanced molecular diversity, with XTD/GA achieving the best performance in goal-directed benchmarks. Furthermore, amine properties were optimized using SAGE-Amine for SPO and MPO tasks. Through iterative fine-tuning, SAGE-Amine demonstrated a progressive improvement in selecting high-scoring amines with desired characteristics such as high basicity, low viscosity, and optimal CO₂ absorption properties. These results underscore SAGE-Amine’s potential for task-specific molecular discovery and its applicability in amine-based CO₂ capture.

This study demonstrated that SAGE-Amine can generate amines with desired properties, but there remains significant room for improvement in this generative approach. First, although the rediscovery task in the goal-directed benchmark suggests that the chemical space SAGE-Amine can explore is vast, the search space narrows due to the reliance on QSPR models for selecting top-ranked amines. To overcome this, it is essential to improve the prediction performance and application domain of QSPR models, as accurate predictions and broad applicability are crucial. Second, the CO₂ absorption MPO task targeted in this study still requires consideration of additional properties beyond those used in this work. These include the CO₂ cyclic capacity, CO₂ absorption rate, heat of reaction with CO₂, corrosion rate, biodegradability, stability, and toxicity. Although the MPO tasks were defined for CO₂ absorption with the available QSPR models, employing a wider range of QSPR models to cover a broader application domain and more desired properties could lead to the discovery of better amines for CO₂ absorption. Third, the NLP models used in this study for pre-training and autoregressive generation were built using a single GPU. The results from large language models (LLMs) indicate that more model parameters and larger pre-training datasets enhance performance [72]. The amine datasets used for pre-training in this study were limited compared to the broader scope of GDB-13, and the NLP models had significantly fewer parameters than other LLMs. Future research should utilize NLP models with more parameters and larger pre-training datasets to achieve better performance.

Efficient CO₂ capture remains a major challenge in combating climate change, requiring improvements in amine-based solvents beyond conventional trial-and-error methods. This study presents SAGE-Amine, a generative framework that combines autoregressive NLP models with QSPR-based optimization to design novel amines for CO₂ absorption. By exploring beyond predefined chemical spaces, SAGE-Amine generates amines with enhanced properties, including higher pKa, lower viscosity, and reduced vapor pressure. The results highlight generative modeling as a powerful tool for accelerating material discovery and optimizing amines for multi-objective criteria. By shifting from traditional screening to de novo molecular design, SAGE-Amine enables the rapid discovery of task-specific chemicals, reducing reliance on costly, time-intensive synthesis. As generative models advance, they are poised to drive the next generation of chemical and material innovation.

5 Author Contributions

H.L. conceptualized and wrote the manuscript. H.C. and J.K. supported making quantitative structure-property relationship models. All authors reviewed the manuscript.

6 Acknowledgments

This research was supported by Quantum Advantage challenge research based on Quantum Computing through the National Research Foundation of Korea (NRF) funded by the Ministry of Science and ICT (RS-2023-00257288). H.L. acknowledges the Computational Systems Biology Laboratory at Yonsei University and Kyoung Tai No for providing access to the COSMOtherm software.

7 Declarations

Competing interests

The authors declare no competing interest.

Funding

H.L., H.C., and J.K. are financially supported by Quantum Advantage challenge research based on Quantum Computing through the National Research Foundation of Korea (NRF) funded by the Ministry of Science and ICT (RS-2023-00257288)..

Code Availability

All results in this work can be found at <https://github.com/hclim0213/SAGE-Amine>.

References

- [1] Rahmanifard, H. and T. Plaksina, Hybrid compressed air energy storage, wind and geothermal energy systems in Alberta: Feasibility simulation and economic assessment. *Renewable Energy*, 2019. 143: p. 453-470.
- [2] Metz, B., O. Davidson, H. De Coninck, M. Loos, and L. Meyer, IPCC special report on carbon dioxide capture and storage. 2005: Cambridge: *Cambridge University Press*.
- [3] Aghel, B., S. Janati, S. Wongwises, and M.S. Shadloo, Review on CO₂ capture by blended amine solutions. *International Journal of Greenhouse Gas Control*, 2022. 119: p. 103715.
- [4] Bernhardsen, I.M. and H.K. Knuutila, A review of potential amine solvents for CO₂ absorption process: Absorption capacity, cyclic capacity and pKa. *International Journal of Greenhouse Gas Control*, 2017. 61: p. 27-48.
- [5] Luis, P., Use of monoethanolamine (MEA) for CO₂ capture in a global scenario: Consequences and alternatives. *Desalination*, 2016. 380: p. 93-99.
- [6] Huttenhuis, P.J.G., N. Agrawal, J. Hogendoorn, and G. Versteeg, Gas solubility of H₂S and CO₂ in aqueous solutions of N-methyldiethanolamine. *Journal of Petroleum Science and Engineering*, 2007. 55(1-2): p. 122-134.
- [7] Wang, X. and B. Li, phase-change solvents for CO₂ capture. *Novel materials for carbon dioxide mitigation technology*, 2015: p. 3-22.
- [8] Rochelle, G., E. Chen, S. Freeman, D. Van Wagener, Q. Xu, and A. Voice, Aqueous piperazine as the new standard for CO₂ capture technology. *Chemical engineering journal*, 2011. 171(3): p. 725-733.
- [9] Svendsen, H.F., E.T. Hessen, and T. Mejdell, Carbon dioxide capture by absorption, challenges and possibilities. *Chemical Engineering Journal*, 2011. 171(3): p. 718-724.
- [10] Aghaie, M., N. Rezaei, and S. Zendehboudi, A systematic review on CO₂ capture with ionic liquids: Current status and future prospects. *Renewable and sustainable energy reviews*, 2018. 96: p. 502-525.
- [11] Hack, J., N. Maeda, and D.M. Meier, Review on CO₂ capture using amine-functionalized materials. *ACS omega*, 2022. 7(44): p. 39520-39530.
- [12] Puxty, G., R. Rowland, A. Allport, Q. Yang, M. Bown, R. Burns, M. Maeder, and M. Attalla, Carbon dioxide postcombustion capture: a novel screening study of the carbon dioxide absorption performance of 76 amines. *Environmental science & technology*, 2009. 43(16): p. 6427-6433.
- [13] El Hadri, N., D.V. Quang, E.L. Goetheer, and M.R.A. Zahra, Aqueous amine solution characterization for post-combustion CO₂ capture process. *Applied Energy*, 2017. 185: p. 1433-1449.

- [14] Fleming, N., How artificial intelligence is changing drug discovery. *Nature*, 2018. 557(7706): p. S55-S55.
- [15] Schütt, K.T., M. Gastegger, A. Tkatchenko, K.-R. Müller, and R.J. Maurer, Unifying machine learning and quantum chemistry with a deep neural network for molecular wavefunctions. *Nature communications*, 2019. 10(1): p. 5024.
- [16] Schneider, P., W.P. Walters, A.T. Plowright, N. Sieroka, J. Listgarten, R.A. Goodnow Jr, J. Fisher, J.M. Jansen, J.S. Duca, and T.S. Rush, Rethinking drug design in the artificial intelligence era. *Nature Reviews Drug Discovery*, 2020. 19(5): p. 353-364.
- [17] Brown, N., M. Fiscato, M.H. Segler, and A.C. Vaucher, GuacaMol: benchmarking models for de novo molecular design. *Journal of chemical information and modeling*, 2019. 59(3): p. 1096-1108.
- [18] Lim, H., Development of scoring-assisted generative exploration (SAGE) and its application to dual inhibitor design for acetylcholinesterase and monoamine oxidase B. *Journal of Cheminformatics*, 2024. 16(1): p. 1-20.
- [19] Lim, H., Development of Scoring-Assisted Generative Exploration (SAGE) and Its Application to Enzyme Inhibitor Design. *Pharmaceutical Research: Recent Advances and Trends Vol. 5*, 2024: p. 145-179.
- [20] Hochreiter, S. and J. Schmidhuber, Long short-term memory. *Neural computation*, 1997. 9(8): p. 1735-1780.
- [21] Graves, A. and A. Graves, Long short-term memory. *Supervised sequence labelling with recurrent neural networks*, 2012: p. 37-45.
- [22] Vaswani, A., N. Shazeer, N. Parmar, J. Uszkoreit, L. Jones, A.N. Gomez, Ł. Kaiser, and I. Polosukhin, Attention is all you need. *Advances in neural information processing systems*, 2017. 30.
- [23] Radford, A., K. Narasimhan, T. Salimans, and I. Sutskever, Improving language understanding by generative pre-training. 2018.
- [24] Wang, P., x-transformers. *GitHub repository*, 2024.
- [25] Burtsev, M.S., Y. Kuratov, A. Peganov, and G.V. Sapunov, Memory transformer. *arXiv preprint arXiv:2006.11527*, 2020.
- [26] Nguyen, T.Q. and J. Salazar, Transformers without tears: Improving the normalization of self-attention. *arXiv preprint arXiv:1910.05895*, 2019.
- [27] Sun, Y., L. Dong, B. Patra, S. Ma, S. Huang, A. Benhaim, V. Chaudhary, X. Song, and F. Wei, A length-extrapolatable transformer. *arXiv preprint arXiv:2212.10554*, 2022.
- [28] Raffel, C., N. Shazeer, A. Roberts, K. Lee, S. Narang, M. Matena, Y. Zhou, W. Li, and P.J. Liu, Exploring the limits of transfer learning with a unified text-to-text transformer. *Journal of machine learning research*, 2020. 21(140): p. 1-67.
- [29] Qin, Z., D. Li, W. Sun, W. Sun, X. Shen, X. Han, Y. Wei, B. Lv, X. Luo, and Y. Qiao, Transormerllm: A faster and better large language model with improved transormer. 2023.
- [30] Yu, T., X. Li, Y. Cai, M. Sun, and P. Li. S2-mlp: Spatial-shift mlp architecture for vision. in *Proceedings of the IEEE/CVF winter conference on applications of computer vision*. 2022.
- [31] Parisotto, E., F. Song, J. Rae, R. Pascanu, C. Gulcehre, S. Jayakumar, M. Jaderberg, R.L. Kaufman, A. Clark, and S. Noury. Stabilizing transformers for reinforcement learning. in *International conference on machine learning*. 2020. PMLR.
- [32] Shleifer, S., J. Weston, and M. Ott, Normformer: Improved transformer pretraining with extra normalization. *arXiv preprint arXiv:2110.09456*, 2021.
- [33] Shazeer, N., Fast transformer decoding: One write-head is all you need. *arXiv preprint arXiv:1911.02150*, 2019.
- [34] Henry, A., P.R. Dachapally, S. Pawar, and Y. Chen, Query-key normalization for transformers. *arXiv preprint arXiv:2010.04245*, 2020.
- [35] Zhao, G., J. Lin, Z. Zhang, X. Ren, Q. Su, and X. Sun, Explicit sparse transformer: Concentrated attention through explicit selection. *arXiv preprint arXiv:1912.11637*, 2019.
- [36] Shazeer, N., Z. Lan, Y. Cheng, N. Ding, and L. Hou, Talking-heads attention. *arXiv preprint arXiv:2003.02436*, 2020.
- [37] Shazeer, N., Glu variants improve transformer. *arXiv preprint arXiv:2002.05202*, 2020.
- [38] Geiping, J. and T. Goldstein. Cramming: Training a Language Model on a single GPU in one day. in *International Conference on Machine Learning*. 2023. PMLR.
- [39] Weininger, D., SMILES, a chemical language and information system. 1. Introduction to methodology and encoding rules. *Journal of chemical information and computer sciences*, 1988. 28(1): p. 31-36.

- [40] Pan, X., H. Wang, C. Li, J.Z. Zhang, and C. Ji, MolGpka: A web server for small molecule p K a prediction using a graph-convolutional neural network. *Journal of Chemical Information and Modeling*, 2021. 61(7): p. 3159-3165.
- [41] Chew, A.K., M. Sender, Z. Kaplan, A. Chandrasekaran, J. Chief Elk, A.R. Browning, H.S. Kwak, M.D. Halls, and M.A.F. Afzal, Advancing material property prediction: using physics-informed machine learning models for viscosity. *Journal of Cheminformatics*, 2024. 16(1): p. 31.
- [42] Kazakov, A., C.D. Muzny, K. Kroenlein, V. Diky, R.D. Chirico, J.W. Magee, I.M. Abdulagatov, and M. Frenkel, NIST/TRC source data archival system: The next-generation data model for storage of thermophysical properties. *International Journal of Thermophysics*, 2012. 33: p. 22-33.
- [43] EPA, U., Estimation programs interface suite™ for Microsoft® windows, v 4.11. *United States Environmental Protection Agency*, Washington, DC, USA, 2012.
- [44] Williams, A.J., C.M. Grulke, J. Edwards, A.D. McEachran, K. Mansouri, N.C. Baker, G. Patlewicz, I. Shah, J.F. Wambaugh, and R.S. Judson, The CompTox Chemistry Dashboard: a community data resource for environmental chemistry. *Journal of cheminformatics*, 2017. 9: p. 1-27.
- [45] Irwin, J.J., K.G. Tang, J. Young, C. Dandarchuluun, B.R. Wong, M. Khurelbaatar, Y.S. Moroz, J. Mayfield, and R.A. Sayle, ZINC20—a free ultralarge-scale chemical database for ligand discovery. *Journal of chemical information and modeling*, 2020. 60(12): p. 6065-6073.
- [46] Landrum, G., RDKit: A software suite for cheminformatics, computational chemistry, and predictive modeling. 2013, *Academic Press Cambridge*.
- [47] Kingma, D.P. and J. Ba, Adam: A method for stochastic optimization. *arXiv preprint arXiv:1412.6980*, 2014. 1: p. 1-15.
- [48] Thomas, M., R.T. Smith, N.M. O’Boyle, C. de Graaf, and A. Bender, Comparison of structure-and ligand-based scoring functions for deep generative models: a GPCR case study. *Journal of cheminformatics*, 2021. 13(1): p. 39.
- [49] Rogers, D. and M. Hahn, Extended-connectivity fingerprints. *Journal of chemical information and modeling*, 2010. 50(5): p. 742-754.
- [50] Francoeur, P.G. and D.R. Koes, SolTranNet—A machine learning tool for fast aqueous solubility prediction. *Journal of chemical information and modeling*, 2021. 61(6): p. 2530-2536.
- [51] Thakkar, A., V. Chadimová, E.J. Bjerrum, O. Engkvist, and J.-L. Reymond, Retrosynthetic accessibility score (RAScore)—rapid machine learned synthesizability classification from AI driven retrosynthetic planning. *Chemical Science*, 2021. 12(9): p. 3339-3349.
- [52] Sanchez-Garcia, R., D. Havasi, G. Takács, M.C. Robinson, F. von Delft, and C.M. Deane, CoPriNet: graph neural networks provide accurate and rapid compound price prediction for molecule prioritisation. *Digital Discovery*, 2023. 2(1): p. 103-111.
- [53] Bolton, E.E., Y. Wang, P.A. Thiessen, and S.H. Bryant, PubChem: integrated platform of small molecules and biological activities, in *Annual reports in computational chemistry*. 2008, Elsevier. p. 217-241.
- [54] Ji, H., H. Deng, H. Lu, and Z. Zhang, Predicting a molecular fingerprint from an electron ionization mass spectrum with deep neural networks. *Analytical Chemistry*, 2020. 92(13): p. 8649-8653.
- [55] Gedeck, P., B. Rohde, and C. Bartels, QSAR-how good is it in practice? Comparison of descriptor sets on an unbiased cross section of corporate data sets. *Journal of chemical information and modeling*, 2006. 46(5): p. 1924-1936.
- [56] Durant, J.L., B.A. Leland, D.R. Henry, and J.G. Nourse, Reoptimization of MDL keys for use in drug discovery. *Journal of chemical information and computer sciences*, 2002. 42(6): p. 1273-1280.
- [57] Carhart, R.E., D.H. Smith, and R. Venkataraghavan, Atom pairs as molecular features in structure-activity studies: definition and applications. *Journal of Chemical Information and Computer Sciences*, 1985. 25(2): p. 64-73.
- [58] Ke, G., Q. Meng, T. Finley, T. Wang, W. Chen, W. Ma, Q. Ye, and T.-Y. Liu, Lightgbm: A highly efficient gradient boosting decision tree. *Advances in neural information processing systems*, 2017. 30.
- [59] Pedregosa, F., G. Varoquaux, A. Gramfort, V. Michel, B. Thirion, O. Grisel, M. Blondel, P. Prettenhofer, R. Weiss, and V. Dubourg, Scikit-learn: Machine learning in Python. *the Journal of machine Learning research*, 2011. 12: p. 2825-2830.
- [60] Brownlee, J., XGBoost With Python: Gradient Boosted Trees with XGBoost and Scikit-Learn. 2016: *Machine Learning Mastery*.

- [61] Yang, K., K. Swanson, W. Jin, C. Coley, P. Eiden, H. Gao, A. Guzman-Perez, T. Hopper, B. Kelley, and M. Mathea, Analyzing learned molecular representations for property prediction. *Journal of chemical information and modeling*, 2019. 59(8): p. 3370-3388.
- [62] Klamt, A. and F. Eckert, COSMO-RS: a novel and efficient method for the a priori prediction of thermophysical data of liquids. *Fluid Phase Equilibria*, 2000. 172(1): p. 43-72.
- [63] Klamt, A., F. Eckert, and W. Arlt, COSMO-RS: an alternative to simulation for calculating thermodynamic properties of liquid mixtures. *Annual review of chemical and biomolecular engineering*, 2010. 1(1): p. 101-122.
- [64] Klamt, A., The COSMO and COSMO-RS solvation models. *Wiley Interdisciplinary Reviews: Computational Molecular Science*, 2011. 1(5): p. 699-709.
- [65] Release, S., LigPrep, Schrödinger, LLC. New York, 2017.
- [66] Steffen, C., K. Thomas, U. Huniar, A. Hellweg, O. Rubner, and A. Schroer, TmoleX—a graphical user interface for TURBOMOLE. *Journal of computational chemistry*, 2010. 31(16): p. 2967-2970.
- [67] Perdew, J.P., Density-functional approximation for the correlation energy of the inhomogeneous electron gas. *Physical review B*, 1986. 33(12): p. 8822.
- [68] Becke, A.D., Density-functional exchange-energy approximation with correct asymptotic behavior. *Physical review A*, 1988. 38(6): p. 3098.
- [69] Grimme, S., J. Antony, S. Ehrlich, and H. Krieg, A consistent and accurate ab initio parametrization of density functional dispersion correction (DFT-D) for the 94 elements H-Pu. *The Journal of chemical physics*, 2010. 132(15).
- [70] Skylaris, C.-K., L. Gagliardi, N.C. Handy, A.G. Ioannou, S. Spencer, and A. Willetts, On the resolution of identity Coulomb energy approximation in density functional theory. *Journal of Molecular Structure: THEOCHEM*, 2000. 501: p. 229-239.
- [71] Khalili, F., A. Rayer, A. Henni, A. East, and P. Tontiwachwuthikul, Kinetics and dissociation constants (pKa) of polyamines of importance in post-combustion carbon dioxide (CO₂) capture studies, in Recent Advances in Post-Combustion CO₂ Capture Chemistry. 2012, *ACS Publications*. p. 43-70.
- [72] Kaplan, J., S. McCandlish, T. Henighan, T.B. Brown, B. Chess, R. Child, S. Gray, A. Radford, J. Wu, and D. Amodei, Scaling laws for neural language models. *arXiv preprint arXiv:2001.08361*, 2020.

SAGE-AMINE: GENERATIVE AMINE DESIGN WITH MULTIPLE-PROPERTY OPTIMIZATION FOR EFFICIENT CO₂ CAPTURE

Hocheol Lim^{*a}, Hyein Cho^b, and Jeonghoon Kim^a

^aBioinformatics and Molecular Design Research Center (BMDRC), Incheon, 21983, Republic of Korea

^bThe Interdisciplinary Graduate Program in Integrative Biotechnology & Translational Medicine, Yonsei University, Incheon, 21983, Republic of Korea

March 5, 2025

* Corresponding author: Hocheol Lim (ihc0213@yonsei.ac.kr)

The supporting information for ‘SAGE-Amine: Generative Amine Design with Multiple-Property Optimization for Efficient CO₂ Capture’ includes Figures S1-S3 for single property optimization results for high pKa, low viscosity, and low vapor pressure, respectively. It also includes Table S1 for performance metrics of the pre-trained models, Table S2 for the hyperparameter tuning procedure, Tables S3-S6 for performance metrics of QSPR models, and Table S7-S8 for predicted properties of amines used in this work.

In this study, there are many abbreviations as follows. 1-(2HE)PP; 1-(2-Hydroxyethyl)piperidine, 1DMA2P; 1-Dimethylamino-2-Propanol, 1M-2PPE; 1-Methyl-2-piperidinemethanol, 1-MPZ; 1-Methylpiperazine, 2-MPZ; 2-Methylpiperazine, 2-PPE; 2-Piperidineethanol, 4DMA1B; 4-Dimethylamino-1-Butanol, AEP; 1-(2-Aminoethyl)Piperazine, AHMPD; 2-Amino-2-Hydroxymethyl-1,3-Propanediol, AMP; 2-Amino-2-Methyl-1-Propanol, BP; Becke–Perdew, CCUS; Carbon Capture, Utilization, and Storage, COSMO-RS; Conductor-like Screening Model for Real Solvents, DA; Diethylamine, DEA; Diethanolamine, DEAE-EO; 2-(2-Diethylaminoethoxy)ethanol, DEEA; N,N-Diethylethanolamine, DETA; Diethylenetriamine, DFT; density functional theory, D-MPNN; Directed message-passing neural network, ECFP; Extended-connectivity fingerprint, EPZ; 1-Ethyl-Piperazine, FCFP; Functional-class fingerprint, GA; Genetic Algorithm, HomoPZ; Homopiperazine, IPA; Isopropylamine, IPAP; 3-(Isopropylamino)Propanol, LGBM; Light Gradient Boosting Machine, LLM; Large Language Model, LSTM; Long-Short-Term Memory, MACCS; Molecular Access System, MDEA; Methyl-diethanolamine, MEA; Monoethanolamine, MPO; Multiple Property Optimization, NLP; Natural Language Processing, PCFP; PubChem Fingerprint, PZ; Piperazine, QSAR; Quantitative Structure-Property Relationship, QSPR; Quantitative Structure-Activity Relationship, RAScore; Retrosynthetic Accessibility score, RF; Random Forest, RI; Resolution of Identity, SAGE; Scoring-Assisted Generative Exploration, SEDiv; Sphere Exclusion Diversity, SMILES; Simplified Molecular Input Line Entry System, SPO; Single Property Optimization, TD; Transformer Decoder, TETA; Triethylenetetramine, VLE; Vapor-Liquid Equilibrium, XGB; Extreme Gradient Boosting, XTD; X-Transformer Decoder.

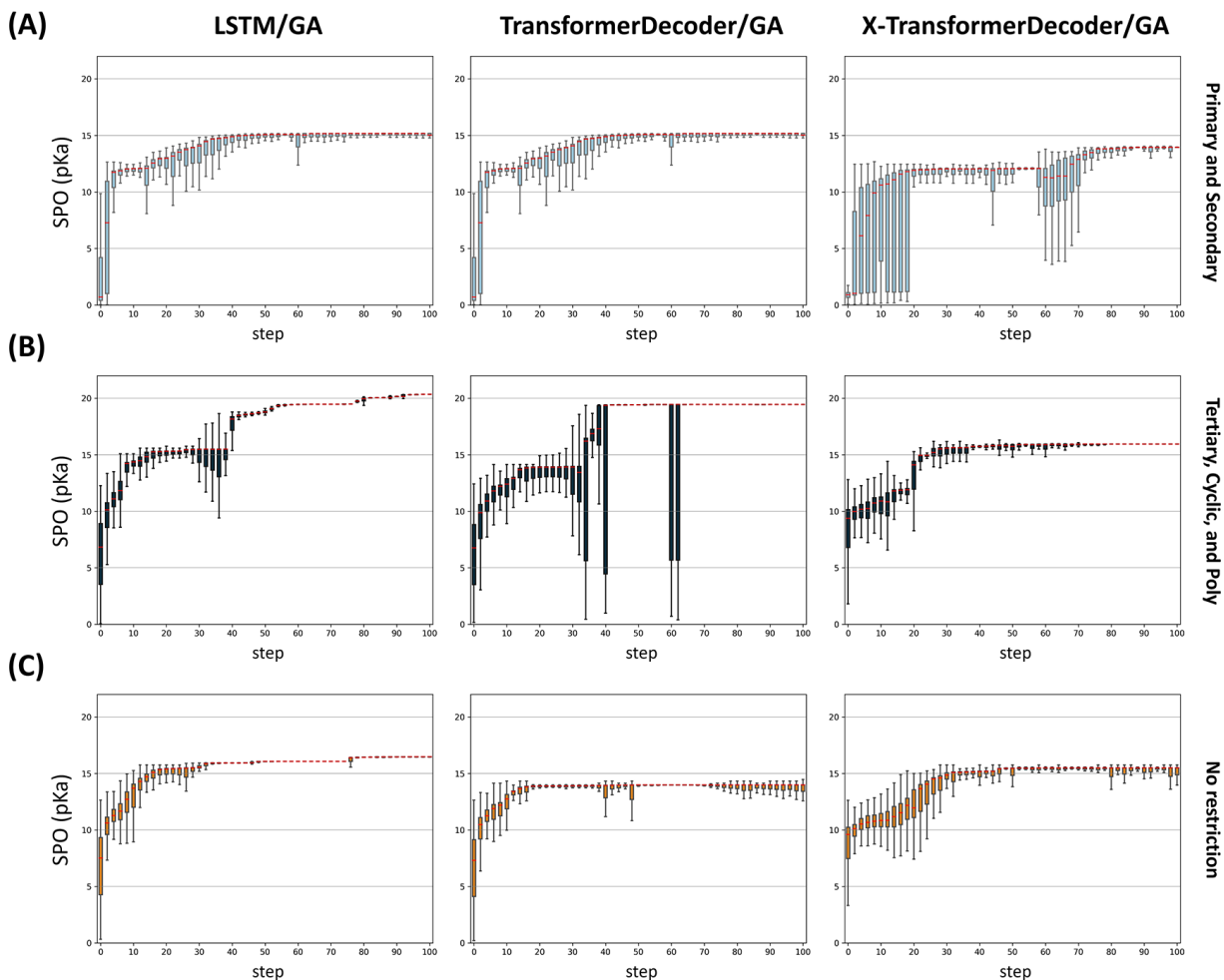


Figure S1: Single-Property Optimization Tasks for Low Viscosity of Amines. (A) Boxplots illustrate the SAGE-Amine process for minimizing viscosity by generating primary and secondary amines using LSTM/GA, TD/GA, and XTD/GA methods. (B) Boxplots depict the generation of tertiary, cyclic, and polyamines for minimizing viscosity. (C) Boxplots represent the steps for generating amines without restrictions on amine type. The medians in each boxplot are highlighted in red.

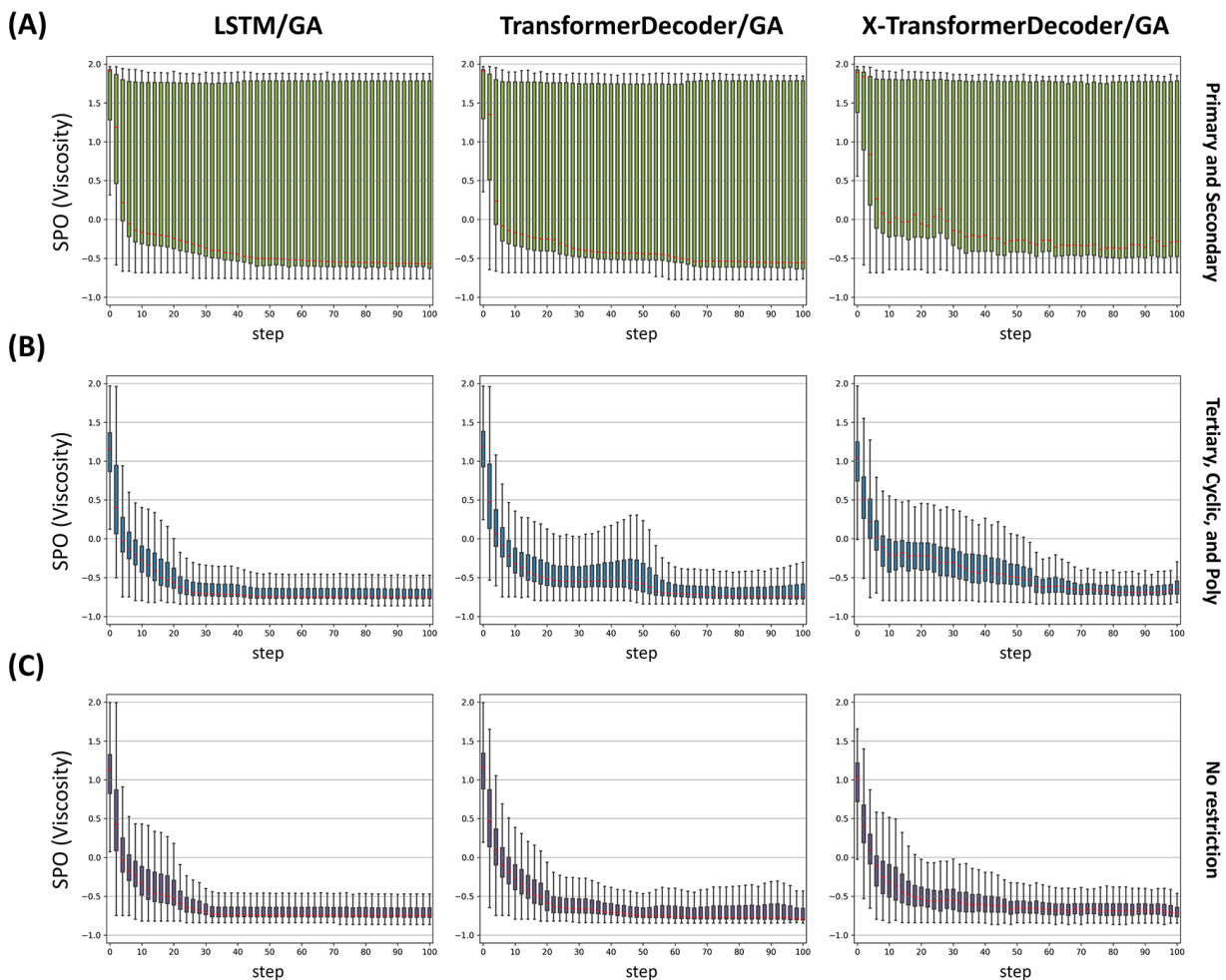


Figure S2: Single-Property Optimization Tasks for High pKa of Amines. (A) Boxplots show the SAGE-Amine process for maximizing pKa through the generation of primary and secondary amines using LSTM/GA, TD/GA, and XTD/GA methods. (B) Boxplots depict the process of generating tertiary, cyclic, and polyamines. (C) Boxplots illustrate the steps for generating amines without restrictions on amine type. The medians in each boxplot are marked in red.

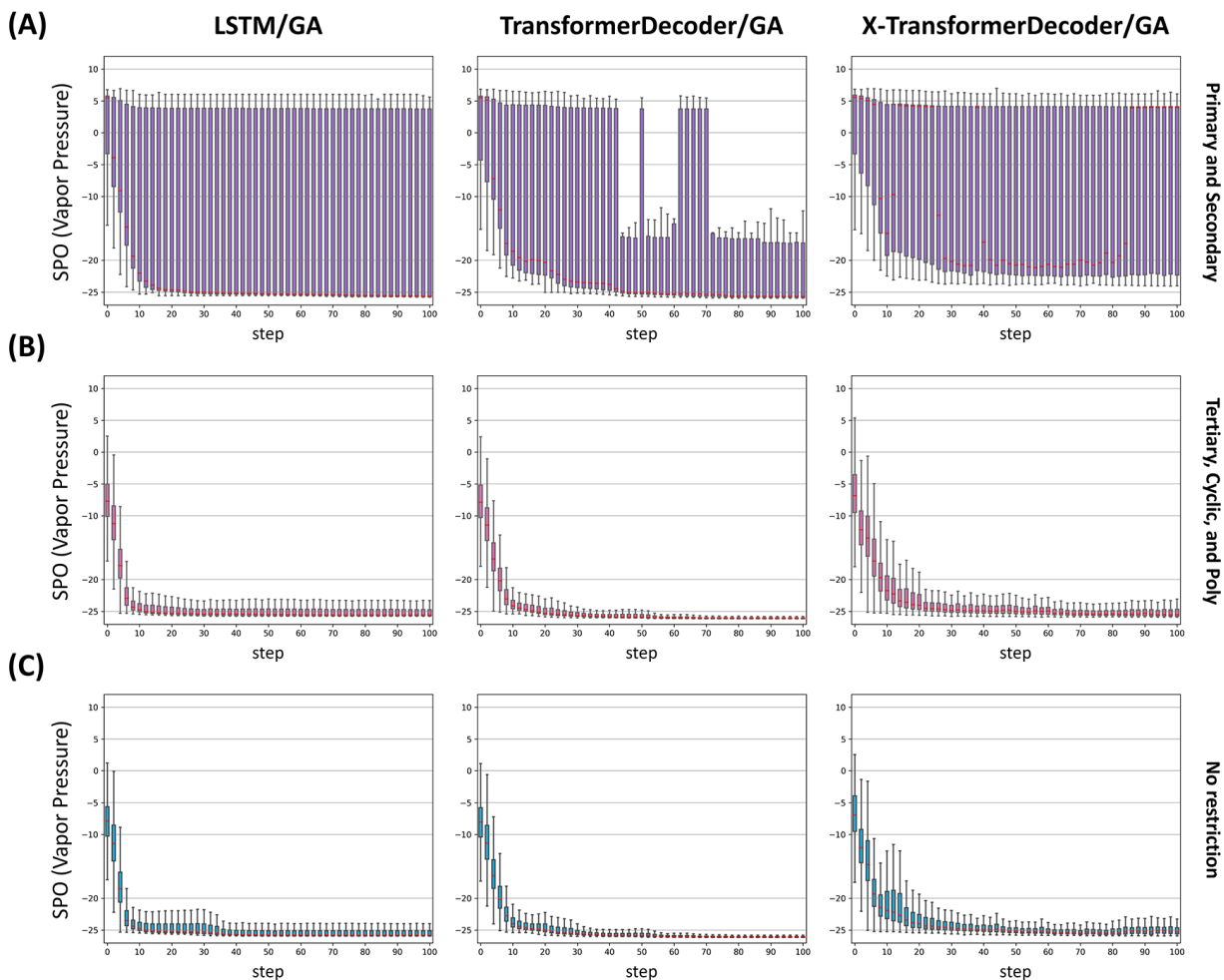


Figure S3: Single-Property Optimization Tasks for Low Vapor Pressure of Amines. (A) Boxplots illustrate the SAGE-Amine process for reducing vapor pressure by generating primary and secondary amines using LSTM/GA, TD/GA, and XTD/GA methods. (B) Boxplots show the generation of tertiary, cyclic, and polyamines aimed at minimizing vapor pressure. (C) Boxplots represent the generation of amines without restrictions on amine type. The medians in each boxplot are highlighted in red.

Table S1: Performance Metrics of Pre-trained Models in this work

Dataset	Models	Samples	Validity	Uniqueness	Novelty	SEDiv	Amine	Primary	Secondary	Tertiary	Cyclic	Poly
Amine250	LSTM	5,000	0.963	0.977	0.502	0.537	0.977	0.068	0.104	0.037	0.666	0.103
		10,000	0.962	0.974	0.494	0.422	0.976	0.068	0.101	0.037	0.668	0.103
	Transformer	5,000	0.972	0.618	0.003	0.387	0.972	0.064	0.106	0.033	0.670	0.099
		10,000	0.974	0.614	0.003	0.311	0.968	0.066	0.109	0.031	0.666	0.095
	TD	5,000	0.962	0.962	0.748	0.517	0.958	0.051	0.092	0.026	0.694	0.095
		10,000	0.962	0.963	0.752	0.411	0.960	0.053	0.096	0.026	0.694	0.092
	XTD	5,000	0.902	0.782	0.733	0.326	0.798	0.033	0.141	0.067	0.275	0.283
		10,000	0.904	0.766	0.722	0.260	0.803	0.031	0.140	0.069	0.271	0.291
	LSTM	5,000	0.962	0.969	0.516	0.540	0.968	0.066	0.110	0.030	0.663	0.101
		10,000	0.963	0.965	0.514	0.425	0.968	0.065	0.108	0.034	0.658	0.103
	Transformer	5,000	0.976	0.609	0.004	0.384	0.969	0.071	0.104	0.038	0.658	0.100
		10,000	0.977	0.607	0.003	0.309	0.967	0.070	0.099	0.037	0.666	0.096
Amine250 reduced	TD	5,000	0.953	0.964	0.746	0.516	0.961	0.058	0.103	0.028	0.688	0.084
		10,000	0.956	0.963	0.748	0.410	0.961	0.059	0.102	0.027	0.686	0.086
	XTD	5,000	0.850	0.772	0.593	0.276	0.976	0.184	0.003	0.000	0.627	0.162
		10,000	0.845	0.710	0.567	0.212	0.974	0.176	0.003	0.000	0.629	0.167
	LSTM	5,000	0.960	0.976	0.765	0.579	0.973	0.030	0.095	0.017	0.738	0.094
		10,000	0.962	0.976	0.767	0.465	0.974	0.026	0.091	0.020	0.742	0.095
	Transformer	5,000	0.978	0.620	0.002	0.400	0.978	0.025	0.109	0.032	0.709	0.103
		10,000	0.979	0.619	0.003	0.331	0.980	0.024	0.108	0.029	0.720	0.099
	TD	5,000	0.961	0.976	0.841	0.525	0.971	0.018	0.092	0.018	0.729	0.114
		10,000	0.962	0.973	0.834	0.416	0.969	0.017	0.101	0.018	0.722	0.110
	XTD	5,000	0.912	0.929	0.910	0.289	0.977	0.002	0.036	0.006	0.473	0.460
		10,000	0.915	0.890	0.872	0.224	0.977	0.002	0.038	0.008	0.473	0.457
Amine300 reduced	LSTM	5,000	0.955	0.980	0.717	0.565	0.978	0.027	0.107	0.029	0.720	0.095
		10,000	0.958	0.977	0.717	0.456	0.976	0.028	0.109	0.027	0.718	0.094
	Transformer	5,000	0.973	0.613	0.003	0.400	0.972	0.028	0.094	0.031	0.723	0.096
		10,000	0.971	0.610	0.003	0.332	0.973	0.030	0.098	0.029	0.717	0.100
	TD	5,000	0.956	0.969	0.829	0.510	0.963	0.020	0.098	0.023	0.721	0.101
		10,000	0.956	0.967	0.822	0.405	0.962	0.019	0.097	0.023	0.718	0.105
	XTD	5,000	0.547	0.986	0.983	0.603	0.987	0.009	0.064	0.014	0.837	0.062
		10,000	0.547	0.979	0.977	0.534	0.988	0.008	0.059	0.013	0.846	0.063

Table S2: Hyperparameters Used in Hyperparameter Tuning Procedure

Method	Tuning Parameters	Fixed Parameters
LGBM	boosting_type = gbdt, dart	
	n_estimators = 100, 500, 1000, 2000, 3000	
	learning_rate = 0.01, 0.05, 0.1	
RF	n_estimators = 100, 500, 1000, 2000, 3000	
	max_depth = 10, 20, 30	
XGB	booster = gbtrees, dart	
	n_estimators = 100, 500, 1000, 2000, 3000	
	max_depth = 10, 20, 30	
	learning_rate = 0.01, 0.05, 0.1	
D-MPNN	hidden_unit = 1024, 2048	learning_rate = 0.001
	step = 1, 2, 4	dropout = 0.1
		num_epochs = 300
		batch_size = 128

Table S3: Mean R-squared from 5-fold Cross-Validation Sets for QSPR Models in Property Optimization Tasks (continued)

Task	Descriptor	Train R-squared				Test R-squared			
		RF	XGB	LGBM	RF	XGB	LGBM		
Viscosity	Avalon	0.9575 \pm 0.0013	0.9533 \pm 0.0009	0.9409 \pm 0.0028	0.8237 \pm 0.0215	0.8262 \pm 0.0183	0.8459 \pm 0.0135		
	ECFP6	0.9692 \pm 0.0009	0.9866 \pm 0.0002	0.9853 \pm 0.0003	0.8396 \pm 0.0199	0.8774 \pm 0.0154	0.8891 \pm 0.0123		
	Extended	0.9577 \pm 0.0022	0.9680 \pm 0.0017	0.9526 \pm 0.0021	0.8258 \pm 0.0222	0.8459 \pm 0.0231	0.8650 \pm 0.0182		
	FCFP4	0.9352 \pm 0.0028	0.9445 \pm 0.0033	0.8944 \pm 0.0041	0.7421 \pm 0.0355	0.7699 \pm 0.0319	0.7573 \pm 0.0227		
	MACCS	0.9599 \pm 0.0013	0.9651 \pm 0.0016	0.9512 \pm 0.0013	0.8530 \pm 0.0211	0.8610 \pm 0.0216	0.8707 \pm 0.0136		
	Morgan	0.9681 \pm 0.0009	0.9897 \pm 0.0005	0.9774 \pm 0.0007	0.8402 \pm 0.0190	0.8808 \pm 0.0214	0.8726 \pm 0.0138		
	PCFP	0.9793 \pm 0.0010	0.9905 \pm 0.0009	0.9857 \pm 0.0009	0.8860 \pm 0.0134	0.9044 \pm 0.0104	0.9199 \pm 0.0110		
	rDesc	0.9904 \pm 0.0004	0.9994 \pm 0.0000	0.9985 \pm 0.0002	0.9345 \pm 0.0078	0.9371 \pm 0.0113	0.9605 \pm 0.0060		
	rPair	0.9760 \pm 0.0009	0.9994 \pm 0.0000	0.9950 \pm 0.0005	0.8892 \pm 0.0125	0.9192 \pm 0.0125	0.9199 \pm 0.0142		
	rTorsion	0.8413 \pm 0.0044	0.9231 \pm 0.0046	0.8054 \pm 0.0021	0.6810 \pm 0.0265	0.7730 \pm 0.0272	0.6508 \pm 0.0162		
	Standard	0.9471 \pm 0.0022	0.9561 \pm 0.0014	0.9367 \pm 0.0013	0.8152 \pm 0.0259	0.8327 \pm 0.0183	0.8457 \pm 0.0141		
	MACCS+Avalon	0.9687 \pm 0.0010	0.9736 \pm 0.0009	0.9725 \pm 0.0010	0.8709 \pm 0.0156	0.8760 \pm 0.0153	0.8929 \pm 0.0097		
MACCS+ECFP6	MACCS+ECFP6	0.9801 \pm 0.0005	0.9912 \pm 0.0005	0.9875 \pm 0.0004	0.8980 \pm 0.0154	0.9057 \pm 0.0137	0.9196 \pm 0.0088		
	MACCS+Extended	0.9713 \pm 0.0013	0.9844 \pm 0.0013	0.9712 \pm 0.0010	0.8657 \pm 0.0162	0.8817 \pm 0.0156	0.8989 \pm 0.0105		
	MACCS+FCFP4	0.9621 \pm 0.0011	0.9691 \pm 0.0014	0.9575 \pm 0.0015	0.8566 \pm 0.0213	0.8645 \pm 0.0229	0.8780 \pm 0.0153		
	MACCS+PCFP	0.9820 \pm 0.0010	0.9928 \pm 0.0005	0.9892 \pm 0.0008	0.9043 \pm 0.0161	0.9136 \pm 0.0132	0.9284 \pm 0.0100		
	MACCS+Standard	0.9723 \pm 0.0011	0.9840 \pm 0.0010	0.9791 \pm 0.0012	0.8739 \pm 0.0180	0.8879 \pm 0.0158	0.8977 \pm 0.0099		

Table S3: Mean R-squared from 5-fold Cross-Validation Sets for QSPR Models in Property Optimization Tasks (continued)

Task	Descriptor	Train R-squared			Test R-squared		
		RF	XGB	LGBM	RF	XGB	LGBM
Boiling Point	Avalon	0.9222 \pm 0.0025	0.9308 \pm 0.0037	0.8755 \pm 0.0074	0.6635 \pm 0.0849	0.6425 \pm 0.0930	0.7114 \pm 0.0543
	ECFP6	0.8988 \pm 0.0041	0.8410 \pm 0.0059	0.7729 \pm 0.0155	0.5122 \pm 0.1357	0.5029 \pm 0.1698	0.6394 \pm 0.0762
	Extended	0.8928 \pm 0.0039	0.9218 \pm 0.0058	0.7981 \pm 0.0147	0.6296 \pm 0.0928	0.6334 \pm 0.1405	0.7020 \pm 0.0608
	FCFP4	0.7374 \pm 0.0223	0.7579 \pm 0.0235	0.7419 \pm 0.0229	0.6234 \pm 0.0655	0.6376 \pm 0.0775	0.6502 \pm 0.0718
	MACCS	0.8777 \pm 0.0044	0.8954 \pm 0.0068	0.7954 \pm 0.0202	0.7389 \pm 0.0260	0.6835 \pm 0.1351	0.7087 \pm 0.0629
	Morgan	0.8943 \pm 0.0038	0.8504 \pm 0.0064	0.8072 \pm 0.0113	0.5317 \pm 0.1565	0.5412 \pm 0.2078	0.6477 \pm 0.0725
	PCFP	0.9176 \pm 0.0066	0.9677 \pm 0.0017	0.8255 \pm 0.0234	0.6621 \pm 0.1039	0.6091 \pm 0.1743	0.7705 \pm 0.0770
	rDesc	0.9731 \pm 0.0016	0.9945 \pm 0.0017	0.9759 \pm 0.0073	0.8373 \pm 0.0475	0.7925 \pm 0.0411	0.8717 \pm 0.0420
	rPair	0.7527 \pm 0.0333	0.8065 \pm 0.0296	0.7711 \pm 0.0319	0.6916 \pm 0.1022	0.7176 \pm 0.1009	0.7239 \pm 0.1067
	rTorsion	0.6716 \pm 0.0323	0.7500 \pm 0.0344	0.7181 \pm 0.0337	0.5990 \pm 0.0949	0.6705 \pm 0.1067	0.6700 \pm 0.1087
	Standard	0.8217 \pm 0.0248	0.8483 \pm 0.0281	0.8179 \pm 0.0277	0.6376 \pm 0.0746	0.6952 \pm 0.0992	0.7067 \pm 0.0868
	MACCS+Avalon	0.9398 \pm 0.0033	0.9737 \pm 0.0020	0.8789 \pm 0.0076	0.7510 \pm 0.0575	0.6890 \pm 0.1643	0.7521 \pm 0.0476
Boiling Point	MACCS+ECFP6	0.9483 \pm 0.0032	0.9832 \pm 0.0017	0.9633 \pm 0.0022	0.7545 \pm 0.0654	0.7826 \pm 0.0432	0.7561 \pm 0.0547
	MACCS+Extended	0.9409 \pm 0.0026	0.9721 \pm 0.0018	0.8835 \pm 0.0108	0.7571 \pm 0.0518	0.7298 \pm 0.1094	0.7626 \pm 0.0570
	MACCS+FCFP4	0.9003 \pm 0.0055	0.9182 \pm 0.0069	0.8157 \pm 0.0199	0.7719 \pm 0.0266	0.7174 \pm 0.1344	0.7420 \pm 0.0636
	MACCS+PCFP	0.9378 \pm 0.0038	0.9803 \pm 0.0017	0.8571 \pm 0.0233	0.7058 \pm 0.0842	0.6907 \pm 0.1516	0.7944 \pm 0.0729
	MACCS+Standard	0.9380 \pm 0.0019	0.9691 \pm 0.0021	0.9144 \pm 0.0084	0.7447 \pm 0.0768	0.7132 \pm 0.1486	0.7457 \pm 0.0786

Table S3: Mean R-squared from 5-fold Cross-Validation Sets for QSPR Models in Property Optimization Tasks (continued)

Task	Descriptor	Train R-squared				Test R-squared			
		RF	XGB	LGBM	RF	XGB	RF	XGB	LGBM
Melting Point	Avalon	0.9197 \pm 0.0020	0.9742 \pm 0.0023	0.9214 \pm 0.0021	0.5275 \pm 0.0911	0.5703 \pm 0.0654	0.5703 \pm 0.0654	0.5703 \pm 0.0654	0.6519 \pm 0.0476
	ECFP6	0.8570 \pm 0.0054	0.8776 \pm 0.0081	0.7510 \pm 0.0159	0.3936 \pm 0.0844	0.4762 \pm 0.0823	0.4762 \pm 0.0823	0.4762 \pm 0.0823	0.5386 \pm 0.0621
	Extended	0.9111 \pm 0.0035	0.9567 \pm 0.0017	0.8561 \pm 0.0221	0.4905 \pm 0.0727	0.5520 \pm 0.0704	0.5520 \pm 0.0704	0.5520 \pm 0.0704	0.6223 \pm 0.0634
	FCFP4	0.7649 \pm 0.0264	0.6908 \pm 0.0218	0.6637 \pm 0.0194	0.4686 \pm 0.0818	0.4543 \pm 0.0833	0.4543 \pm 0.0833	0.4543 \pm 0.0833	0.5294 \pm 0.0639
	MACCS	0.9166 \pm 0.0068	0.9140 \pm 0.0068	0.8400 \pm 0.0137	0.6824 \pm 0.0561	0.6926 \pm 0.0543	0.6926 \pm 0.0543	0.6926 \pm 0.0543	0.6968 \pm 0.0522
	Morgan	0.8946 \pm 0.0056	0.8226 \pm 0.0048	0.7614 \pm 0.0152	0.3515 \pm 0.1464	0.4437 \pm 0.0901	0.4437 \pm 0.0901	0.4437 \pm 0.0901	0.5555 \pm 0.0628
	PCFP	0.9052 \pm 0.0054	0.9063 \pm 0.0035	0.8063 \pm 0.0254	0.5272 \pm 0.0767	0.5713 \pm 0.0678	0.5713 \pm 0.0678	0.5713 \pm 0.0678	0.6255 \pm 0.0680
	rDesc	0.9577 \pm 0.0036	1.0000 \pm 0.0000	0.9405 \pm 0.0069	0.6751 \pm 0.1127	0.6940 \pm 0.1176	0.6940 \pm 0.1176	0.6940 \pm 0.1176	0.7033 \pm 0.0610
	rPair	0.7505 \pm 0.0375	0.7734 \pm 0.0423	0.7329 \pm 0.0380	0.5578 \pm 0.0907	0.5584 \pm 0.0957	0.5584 \pm 0.0957	0.5584 \pm 0.0957	0.5763 \pm 0.0908
	rTorsion	0.5518 \pm 0.0299	0.6199 \pm 0.0360	0.5379 \pm 0.0288	0.3594 \pm 0.0667	0.3787 \pm 0.0690	0.3787 \pm 0.0690	0.3787 \pm 0.0690	0.4442 \pm 0.0759
	Standard	0.7318 \pm 0.0214	0.8575 \pm 0.0270	0.8153 \pm 0.0295	0.4800 \pm 0.0468	0.5317 \pm 0.0790	0.5317 \pm 0.0790	0.5317 \pm 0.0790	0.5877 \pm 0.0807
	MACCS+Avalon	0.9526 \pm 0.0030	0.9912 \pm 0.0007	0.9091 \pm 0.0038	0.6672 \pm 0.0607	0.6856 \pm 0.0667	0.6856 \pm 0.0667	0.6856 \pm 0.0667	0.6983 \pm 0.0555
	MACCS+ECFP6	0.9540 \pm 0.0027	0.9759 \pm 0.0006	0.8852 \pm 0.0064	0.6867 \pm 0.0544	0.7052 \pm 0.0368	0.7052 \pm 0.0368	0.7052 \pm 0.0368	0.7130 \pm 0.0477
	MACCS+Extended	0.9557 \pm 0.0021	0.9652 \pm 0.0009	0.9273 \pm 0.0087	0.6974 \pm 0.0292	0.7080 \pm 0.0163	0.7080 \pm 0.0163	0.7080 \pm 0.0163	0.7190 \pm 0.0515
	MACCS+FCFP4	0.9375 \pm 0.0069	0.9220 \pm 0.0073	0.8682 \pm 0.0152	0.7021 \pm 0.0536	0.7090 \pm 0.0521	0.7090 \pm 0.0521	0.7090 \pm 0.0521	0.7115 \pm 0.0571
	MACCS+PCFP	0.9533 \pm 0.0028	0.9645 \pm 0.0022	0.8900 \pm 0.0145	0.7004 \pm 0.0273	0.7337 \pm 0.0363	0.7337 \pm 0.0363	0.7337 \pm 0.0363	0.7289 \pm 0.0557
	MACCS+Standard	0.9491 \pm 0.0045	0.9617 \pm 0.0035	0.8281 \pm 0.0084	0.6871 \pm 0.0471	0.7113 \pm 0.0387	0.7113 \pm 0.0387	0.7113 \pm 0.0387	0.6857 \pm 0.0494

Table S4: Mean Absolute Error from 5-fold Cross-Validation Sets for QSPR Models in Property Optimization Tasks (continued)

Task	Descriptor	Train MAE			Test MAE		
		RF	XGB	LGBM	RF	XGB	LGBM
Viscosity	Avalon	0.0522 \pm 0.0008	0.0492 \pm 0.0010	0.0626 \pm 0.0014	0.1144 \pm 0.0073	0.1202 \pm 0.0062	0.1141 \pm 0.0055
	ECFP6	0.0493 \pm 0.0005	0.0264 \pm 0.0006	0.0304 \pm 0.0005	0.1100 \pm 0.0056	0.0946 \pm 0.0075	0.0937 \pm 0.0062
	Extended	0.0520 \pm 0.0009	0.0391 \pm 0.0011	0.0575 \pm 0.0010	0.1128 \pm 0.0049	0.1068 \pm 0.0054	0.1032 \pm 0.0049
	FCFP4	0.0726 \pm 0.0011	0.0585 \pm 0.0016	0.1011 \pm 0.0021	0.1532 \pm 0.0088	0.1468 \pm 0.0095	0.1593 \pm 0.0076
	MACCS	0.0531 \pm 0.0010	0.0440 \pm 0.0010	0.0608 \pm 0.0006	0.1105 \pm 0.0074	0.1081 \pm 0.0075	0.1061 \pm 0.0067
	Morgan	0.0503 \pm 0.0006	0.0186 \pm 0.0002	0.0420 \pm 0.0013	0.1104 \pm 0.0043	0.0913 \pm 0.0071	0.1009 \pm 0.0050
	PCFP	0.0390 \pm 0.0009	0.0202 \pm 0.0007	0.0320 \pm 0.0007	0.0930 \pm 0.0050	0.0852 \pm 0.0051	0.0805 \pm 0.0045
	rDesc	0.0247 \pm 0.0002	0.0028 \pm 0.0001	0.0105 \pm 0.0006	0.0640 \pm 0.0034	0.0594 \pm 0.0031	0.0468 \pm 0.0023
	rPair	0.0436 \pm 0.0009	0.0037 \pm 0.0001	0.0165 \pm 0.0004	0.0902 \pm 0.0030	0.0688 \pm 0.0046	0.0722 \pm 0.0060
	rTorsion	0.1239 \pm 0.0017	0.0681 \pm 0.0019	0.1313 \pm 0.0008	0.1782 \pm 0.0082	0.1364 \pm 0.0069	0.1885 \pm 0.0053
	Standard	0.0619 \pm 0.0010	0.0490 \pm 0.0003	0.0701 \pm 0.0009	0.1239 \pm 0.0045	0.1168 \pm 0.0037	0.1155 \pm 0.0035
	MACCS+Avalon	0.0437 \pm 0.0006	0.0350 \pm 0.0005	0.0367 \pm 0.0006	0.0972 \pm 0.0065	0.0985 \pm 0.0070	0.0916 \pm 0.0047
	MACCS+ECFP6	0.0368 \pm 0.0003	0.0175 \pm 0.0007	0.0271 \pm 0.0005	0.0874 \pm 0.0047	0.0820 \pm 0.0027	0.0768 \pm 0.0044
	MACCS+Extended	0.0424 \pm 0.0008	0.0214 \pm 0.0006	0.0421 \pm 0.0007	0.0982 \pm 0.0046	0.0906 \pm 0.0045	0.0854 \pm 0.0032
	MACCS+FCFP4	0.0518 \pm 0.0010	0.0387 \pm 0.0012	0.0548 \pm 0.0006	0.1069 \pm 0.0075	0.1026 \pm 0.0069	0.1007 \pm 0.0064
	MACCS+PCFP	0.0362 \pm 0.0008	0.0161 \pm 0.0005	0.0257 \pm 0.0004	0.0869 \pm 0.0064	0.0797 \pm 0.0044	0.0735 \pm 0.0044
	MACCS+Standard	0.0415 \pm 0.0008	0.0219 \pm 0.0003	0.0327 \pm 0.0008	0.0957 \pm 0.0050	0.0897 \pm 0.0059	0.0861 \pm 0.0033

Table S4: Mean Absolute Error from 5-fold Cross-Validation Sets for QSPR Models in Property Optimization Tasks (continued)

Task	Descriptor	Train MAE			Test MAE		
		RF	XGB	LGBM	RF	XGB	LGBM
Vapor Pressure	Avalon	0.4692 \pm 0.0088	0.1985 \pm 0.0102	0.4304 \pm 0.0100	1.0501 \pm 0.0681	1.0450 \pm 0.0520	1.0088 \pm 0.0602
	ECFP6	0.5651 \pm 0.0148	0.1775 \pm 0.0063	0.5391 \pm 0.0094	1.2634 \pm 0.0440	1.2401 \pm 0.0309	1.1910 \pm 0.0494
	Extended	0.4584 \pm 0.0125	0.1496 \pm 0.0067	0.4280 \pm 0.0125	0.9944 \pm 0.0756	0.9947 \pm 0.0637	0.9589 \pm 0.0491
	FCFP4	0.6517 \pm 0.0175	0.6963 \pm 0.0231	0.7441 \pm 0.0164	1.3300 \pm 0.0905	1.3173 \pm 0.0714	1.3031 \pm 0.0683
	MACCS	0.5286 \pm 0.0101	0.3010 \pm 0.0099	0.7654 \pm 0.0103	1.0599 \pm 0.0444	1.0588 \pm 0.0349	1.0414 \pm 0.0492
	Morgan	0.5679 \pm 0.0162	0.1401 \pm 0.0062	0.6175 \pm 0.0149	1.2547 \pm 0.0482	1.2341 \pm 0.0307	1.1802 \pm 0.0463
	PCFP	0.3609 \pm 0.0064	0.1956 \pm 0.0072	0.5857 \pm 0.0158	0.8490 \pm 0.0542	0.8208 \pm 0.0411	0.8344 \pm 0.0405
	rDesc	0.2520 \pm 0.0038	0.0041 \pm 0.0010	0.1438 \pm 0.0059	0.6859 \pm 0.0466	0.6833 \pm 0.0548	0.6332 \pm 0.0386
	rPair	0.4027 \pm 0.0088	0.0298 \pm 0.0024	0.3212 \pm 0.0106	0.9009 \pm 0.0495	0.8180 \pm 0.0343	0.8178 \pm 0.0448
	rTorsion	0.8364 \pm 0.0126	0.2559 \pm 0.0103	0.9203 \pm 0.0196	1.3625 \pm 0.0537	1.1543 \pm 0.0569	1.2874 \pm 0.0614
	Standard	0.5128 \pm 0.0129	0.1897 \pm 0.0118	0.5500 \pm 0.0156	1.0766 \pm 0.0614	1.0628 \pm 0.0680	1.0344 \pm 0.0611
	MACCS+Avalon	0.4119 \pm 0.0090	0.1430 \pm 0.0101	0.4192 \pm 0.0107	0.9417 \pm 0.0617	0.9327 \pm 0.0497	0.8920 \pm 0.0537
Vapor Pressure	MACCS+ECFP6	0.4066 \pm 0.0078	0.0780 \pm 0.0064	0.4506 \pm 0.0058	0.9774 \pm 0.0413	0.9410 \pm 0.0413	0.9105 \pm 0.0471
	MACCS+Extended	0.4005 \pm 0.0086	0.1132 \pm 0.0068	0.3525 \pm 0.0084	0.9269 \pm 0.0361	0.8974 \pm 0.0361	0.8536 \pm 0.0382
	MACCS+FCFP4	0.4408 \pm 0.0083	0.1565 \pm 0.0074	0.5575 \pm 0.0119	1.0008 \pm 0.0472	0.9832 \pm 0.0469	0.9600 \pm 0.0493
	MACCS+PCFP	0.3379 \pm 0.0043	0.1405 \pm 0.0036	0.5140 \pm 0.0115	0.8278 \pm 0.0435	0.8046 \pm 0.0330	0.7909 \pm 0.0354
	MACCS+Standard	0.4231 \pm 0.0079	0.1770 \pm 0.0078	0.4443 \pm 0.0072	0.9564 \pm 0.0318	0.9289 \pm 0.0346	0.9045 \pm 0.0474

Table S4: Mean Absolute Error from 5-fold Cross-Validation Sets for QSPR Models in Property Optimization Tasks (continued)

Task	Descriptor	Train MAE			Test MAE		
		RF	XGB	LGBM	RF	XGB	LGBM
Boiling Point	Avalon	17.3877 \pm 0.1726	20.0135 \pm 0.1161	26.0231 \pm 0.3516	32.8276 \pm 1.1045	34.1708 \pm 1.0398	35.1695 \pm 0.6493
	ECFP6	24.4987 \pm 0.2474	30.5057 \pm 0.4642	30.0908 \pm 0.6461	42.0744 \pm 0.9848	42.6827 \pm 1.4124	39.5387 \pm 0.6686
	Extended	23.0221 \pm 0.2164	21.6051 \pm 0.1174	27.8535 \pm 0.4074	34.2761 \pm 1.1223	32.6260 \pm 1.1903	33.5599 \pm 0.7087
	FCFP4	32.0229 \pm 0.3083	23.9116 \pm 0.3165	30.5974 \pm 0.3569	45.5891 \pm 1.1837	42.0005 \pm 1.2836	43.0536 \pm 1.2299
	MACCS	21.4766 \pm 0.1654	17.4496 \pm 0.1401	25.6455 \pm 0.3146	34.2512 \pm 0.5930	32.9908 \pm 0.6604	34.4723 \pm 0.6426
	Morgan	26.3002 \pm 0.2665	31.9553 \pm 0.3493	28.9075 \pm 0.5342	42.3722 \pm 1.1009	42.2758 \pm 1.1023	38.3494 \pm 0.6076
	PCFP	20.3719 \pm 0.5296	15.5003 \pm 0.3272	18.3211 \pm 0.3023	29.8851 \pm 0.6985	26.4832 \pm 0.9790	24.3217 \pm 0.8834
	rDesc	6.6924 \pm 0.0830	4.1586 \pm 0.1406	8.0413 \pm 0.2153	16.3748 \pm 0.5560	14.9647 \pm 0.5258	14.8977 \pm 0.5842
	rPair	15.6009 \pm 0.5103	6.0165 \pm 0.4301	13.6085 \pm 0.5235	26.1700 \pm 0.7893	22.7767 \pm 1.0517	20.9254 \pm 0.9880
	rTorsion	32.3111 \pm 0.4193	11.4244 \pm 0.3928	19.6784 \pm 0.4212	42.0223 \pm 0.9321	27.3570 \pm 1.1061	29.5150 \pm 0.9795
	Standard	28.1876 \pm 0.2905	20.8710 \pm 0.2774	24.7708 \pm 0.3872	38.7724 \pm 0.8570	33.6532 \pm 0.9018	33.4765 \pm 0.6688
	MACCS+Avalon	14.3461 \pm 0.0902	8.6000 \pm 0.0635	23.8060 \pm 0.2380	27.6977 \pm 0.5893	25.4484 \pm 0.8306	29.3114 \pm 0.6240
Boiling Point	MACCS+ECFP6	14.6715 \pm 0.0718	5.3615 \pm 0.0365	13.3142 \pm 0.1921	29.1097 \pm 0.7841	24.5718 \pm 0.5995	27.5992 \pm 0.7809
	MACCS+Extended	14.2221 \pm 0.0996	9.1373 \pm 0.0861	20.7150 \pm 0.2979	26.9891 \pm 0.7866	25.4066 \pm 0.8132	26.7427 \pm 0.6741
	MACCS+FCFP4	17.2982 \pm 0.1390	12.1720 \pm 0.1412	21.6963 \pm 0.2631	30.5750 \pm 0.6446	29.1147 \pm 0.6753	29.2181 \pm 0.7360
	MACCS+PCFP	16.8144 \pm 0.3174	12.4125 \pm 0.4001	13.1975 \pm 0.2459	26.5555 \pm 0.9004	22.0956 \pm 0.7377	21.3474 \pm 0.8277
	MACCS+Standard	15.0954 \pm 0.1055	9.0461 \pm 0.1260	18.4586 \pm 0.1537	28.4801 \pm 1.0979	25.4917 \pm 0.7915	26.9618 \pm 0.6092

Table S4: Mean Absolute Error from 5-fold Cross-Validation Sets for QSPR Models in Property Optimization Tasks (continued)

Task	Descriptor	Train MAE			Test MAE		
		RF	XGB	LGBM	RF	XGB	LGBM
Melting Point	Avalon	18.9529 \pm 0.2190	11.0297 \pm 0.3442	21.6631 \pm 0.2782	42.0073 \pm 1.2201	40.7917 \pm 0.9321	38.5489 \pm 0.6548
	ECFP6	27.5477 \pm 0.3684	24.4285 \pm 0.4235	32.0360 \pm 0.5225	48.2928 \pm 1.2862	46.2857 \pm 1.2494	45.7972 \pm 1.2585
	Extended	19.8196 \pm 0.2086	15.6583 \pm 0.3000	21.8304 \pm 0.5045	41.5633 \pm 1.2805	40.2498 \pm 1.6281	38.8988 \pm 1.3600
	FCFP4	25.3407 \pm 0.2453	32.5568 \pm 0.3021	35.9154 \pm 0.3061	47.1176 \pm 1.4401	47.3897 \pm 1.3207	45.6431 \pm 1.3358
	MACCS	19.4993 \pm 0.2957	20.9204 \pm 0.7916	27.1396 \pm 0.2325	39.5261 \pm 1.0891	38.6089 \pm 0.9812	38.2426 \pm 0.9642
	Morgan	22.0873 \pm 0.2921	31.8504 \pm 0.3893	31.7288 \pm 0.5407	46.6470 \pm 1.3454	47.2710 \pm 1.3560	44.5562 \pm 0.9840
	PCFP	20.5629 \pm 0.5395	27.0725 \pm 1.1841	23.6958 \pm 0.2525	39.5804 \pm 0.6510	39.7526 \pm 0.9859	36.6846 \pm 1.3655
	rDesc	13.3164 \pm 0.1626	0.0058 \pm 0.0009	16.1765 \pm 0.2090	34.9355 \pm 1.4013	33.2154 \pm 1.6414	32.8580 \pm 0.8935
	rPair	18.7145 \pm 0.2305	13.4388 \pm 0.5278	21.3272 \pm 0.5309	40.0527 \pm 0.9357	39.3359 \pm 1.2217	38.1215 \pm 1.0678
	rTorsion	38.1780 \pm 0.4031	32.6250 \pm 0.2571	34.2105 \pm 0.3135	53.8855 \pm 1.1296	49.2769 \pm 0.8152	46.6932 \pm 0.9255
	Standard	39.5215 \pm 0.3954	23.7663 \pm 0.1541	23.5328 \pm 0.2843	48.8940 \pm 0.5872	43.7250 \pm 0.9898	41.2393 \pm 1.1467
	MACCS+Avalon	14.7519 \pm 0.0882	6.5527 \pm 0.4285	23.0656 \pm 0.3470	37.4801 \pm 0.7978	35.9206 \pm 0.7576	35.5227 \pm 0.7795
Melting Point	MACCS+ECFP6	14.7570 \pm 0.1204	13.2372 \pm 0.4674	24.2530 \pm 0.3495	37.2167 \pm 0.9317	36.3039 \pm 0.6946	35.9733 \pm 0.7623
	MACCS+Extended	14.5095 \pm 0.1376	15.5373 \pm 0.5970	17.7796 \pm 0.3612	36.5525 \pm 0.9622	35.7252 \pm 0.7057	34.3025 \pm 1.0332
	MACCS+FCFP4	15.4036 \pm 0.2403	20.9573 \pm 0.6580	22.8898 \pm 0.2659	36.9120 \pm 1.1305	37.0774 \pm 0.7197	35.2945 \pm 0.8894
	MACCS+PCFP	13.9686 \pm 0.1342	16.1028 \pm 0.7215	19.3201 \pm 0.2444	35.5762 \pm 0.8548	34.3065 \pm 0.8874	33.2599 \pm 1.0821
	MACCS+Standard	14.9254 \pm 0.1279	15.1921 \pm 0.4789	29.0459 \pm 0.2215	37.3068 \pm 0.8725	36.2012 \pm 0.5919	36.9388 \pm 0.9093

Table S5: Model Performance from 5-fold Cross-Validation Sets for Graph-based D-MPNN

Model	Task	Train R-squared	Train MAE	Test R-squared	Test MAE
Graph/D-MPNN	Viscosity	0.9070 ± 0.0199	0.1150 ± 0.0121	0.9609 ± 0.0187	0.0666 ± 0.0227
	Vapor pressure	0.9891 ± 0.0033	0.2573 ± 0.0247	0.9952 ± 0.0008	0.2016 ± 0.0586
	Boiling Point	0.9806 ± 0.0075	12.1769 ± 0.7928	0.9848 ± 0.0056	21.2934 ± 5.3825
	Melting Point	0.9793 ± 0.0040	13.9387 ± 3.3526	0.9551 ± 0.0187	18.9523 ± 4.1407

Table S6: Performance metrics of the best-found QSPR models for tasks

Task	Model	Train R-squared	Train MAE	Test R-squared	Test MAE
Viscosity	rDesc/LGBM	0.9985 ± 0.0002	0.0105 ± 0.0006	0.9605 ± 0.0060	0.0468 ± 0.0023
Vapor Pressure	Graph/D-MPNN	0.9891 ± 0.0033	0.2573 ± 0.0247	0.9952 ± 0.0008	0.2016 ± 0.0586
Boiling Point	Graph/D-MPNN	0.9806 ± 0.0075	12.1769 ± 0.7928	0.9848 ± 0.0056	21.2934 ± 5.3825
Melting Point	Graph/D-MPNN	0.9793 ± 0.0040	13.9387 ± 3.3526	0.9551 ± 0.0187	18.9523 ± 4.1407

Table S7: Predicted Properties of Amines Used in this work

Amine Type	Name	Molecular Weight	pKa	Viscosity	Vapor Pressure	Boiling Point	Melting Point	RA score	Price	Aqueous Solubility
Primary	MEA	61.084	9.160	0.728	-0.438	132.005	-3.635	0.991	3.035	1.690
	AHMPD	121.136	7.637	1.185	-6.003	326.387	125.803	0.987	4.887	1.010
	AMP	89.138	8.817	0.643	-1.777	154.140	19.075	0.981	4.323	1.267
	IPA	59.112	2.814	-0.429	2.734	45.598	-93.031	0.987	4.004	1.692
	SAGE-01	130.231	11.793	0.718	-3.901	207.633	-50.750	0.953	4.680	0.333
	SAGE-02	103.163	10.538	0.142	-0.920	221.044	-3.753	0.991	2.723	0.706
Secondary	DEA	105.137	9.096	1.261	-2.993	253.185	-14.309	0.994	2.515	1.247
	DA	73.139	1.795	-0.512	2.339	42.306	-79.072	0.992	3.244	1.239
	IPAP	117.192	9.936	0.748	-1.402	186.172	-19.294	0.993	3.077	0.693
	SAGE-03	100.162	11.912	0.521	-2.778	166.675	15.283	0.868	4.449	0.961
	SAGE-04	160.260	11.000	0.386	-3.240	260.011	25.658	0.984	4.312	0.905
	MDEA	119.164	7.969	0.940	-2.764	237.189	-15.973	0.995	4.244	0.985
Tertiary	DEEA	117.192	8.163	0.501	-0.172	155.978	-33.024	0.990	3.842	0.762
	4DMA1B	117.192	9.302	0.651	0.568	165.326	-29.512	0.990	4.401	0.788
	1DMA2P	103.165	8.401	0.387	0.036	122.668	-66.949	0.986	3.931	1.080
	DEAE-EO	161.245	8.429	0.559	-0.847	224.180	-28.831	0.991	5.068	0.389
	SAGE-05	159.272	10.722	0.317	-2.945	677.109	27.061	0.969	4.383	0.299
	SAGE-06	145.246	11.030	0.287	-2.045	239.905	-42.911	0.963	4.384	0.576
Cyclic	2-MPZ	100.165	10.178	0.435	0.474	128.757	62.466	0.980	5.769	1.085
	2-PPE	129.203	10.222	1.260	-1.460	210.111	36.302	0.984	4.941	0.386
	HomoPZ	100.165	10.995	0.516	1.185	88.906	128.928	0.945	6.405	1.115
	1M-2PPE	129.203	9.648	1.073	-0.067	208.248	55.987	0.988	4.540	0.433
	EPZ	114.192	9.508	0.258	-0.011	156.735	4.751	0.990	3.977	0.907
	PZ	86.138	10.461	0.470	-0.179	96.078	-5.808	0.975	5.796	1.181
Poly	1-MPZ	100.165	9.502	0.219	0.542	123.059	-1.550	0.984	4.968	0.924
	AEP	129.207	9.622	0.485	-1.270	221.794	71.807	0.990	4.236	0.838
	1-(2HE)PP	129.203	9.252	0.915	-1.241	193.568	53.934	0.982	4.894	0.456
	SAGE-07	170.255	13.256	0.391	-3.951	177.763	28.361	0.954	5.101	-0.358
	SAGE-08	170.255	13.672	0.448	-1.343	210.015	36.368	0.986	5.225	-0.383
	DETA	103.169	10.272	0.818	-1.234	204.826	26.278	0.964	4.096	1.386
Poly	TETA	146.238	10.364	0.626	-3.424	277.009	117.589	0.968	4.465	1.118
	SAGE-09	158.245	13.127	0.449	-1.168	236.530	0.726	0.956	4.840	0.436
	SAGE-10	158.245	12.859	0.375	-3.155	250.238	63.089	0.968	4.454	0.709

Table S8: COSMO-RS Results of Amines Used in this work

Amine Type	Name	Molecular Weight	CO ₂ Henry's Law Constant	CO ₂ Solubility	Flash Point	Vaporization ΔH	Excess ΔH	Excess ΔG
Primary	MEA	61.084	345.911	-3.045	128.346	51.581	-0.989	-0.319
	AHMPD	121.136	440.125	-3.150	234.885	52.148	-0.351	-0.048
	AMP	89.138	312.544	-3.002	137.628	51.082	-0.573	0.047
	IPA	59.112	222.534	-2.854	-19.444	48.847	-0.875	0.216
	SAGE-01	130.231	279.746	-2.955	88.115	50.255	-0.680	0.130
	SAGE-02	103.163	254.988	-2.915	48.431	50.032	-0.827	0.098
Secondary	DEA	105.137	359.695	-3.063	216.388	52.541	-0.998	-0.272
	DA	73.139	206.572	-2.823	-14.443	48.984	-0.716	0.505
	IPAP	117.192	270.021	-2.940	118.481	50.529	-0.274	0.374
	SAGE-03	100.162	284.207	-2.961	88.682	50.365	-0.597	0.138
	SAGE-04	160.260	278.798	-2.955	145.767	51.109	-1.109	-0.108
	MDEA	119.164	329.834	-3.025	165.051	51.214	-0.386	0.187
Tertiary	DEEA	117.192	265.029	-2.932	86.602	50.088	-0.295	0.473
	4DMA1B	117.192	261.044	-2.925	98.842	50.419	-0.459	0.369
	1DMA2P	103.165	249.698	-2.906	36.519	49.507	-0.615	0.354
	DEAE-EO	161.245	284.424	-2.963	123.121	50.122	-0.180	0.447
	SAGE-05	159.272	261.068	-2.927	112.541	50.370	-0.744	0.143
	SAGE-06	145.246	265.298	-2.933	85.482	50.463	-0.834	0.149
Cyclic	2-MPZ	100.165	273.125	-2.944	64.691	50.489	-1.156	-0.049
	2-PPE	129.203	290.767	-2.972	150.194	50.651	-0.273	0.285
	HomoPZ	100.165	277.481	-2.951	69.746	50.433	-1.096	-0.082
	1M-2PPE	129.203	288.993	-2.969	128.004	50.410	-0.264	0.387
	EPZ	114.192	260.808	-2.925	63.932	50.302	-1.010	0.129
	PZ	86.138	280.012	-2.954	55.932	50.442	-1.238	-0.161
Poly	1-MPZ	100.165	264.517	-2.930	50.912	50.285	-1.151	0.065
	AEP	129.207	296.656	-2.981	127.301	51.431	-1.518	-0.424
	1-(2HE)PP	129.203	282.591	-2.960	121.231	50.400	-0.340	0.358
	SAGE-07	170.255	294.048	-2.978	153.061	50.671	-0.780	-0.021
	SAGE-08	170.255	290.983	-2.974	158.541	50.689	-0.711	-0.005
	DETA	103.169	297.854	-2.981	126.789	51.966	-1.867	-0.788
Poly	TETA	146.238	293.344	-2.976	155.761	51.878	-1.544	-0.533
	SAGE-09	158.245	286.817	-2.967	178.189	50.958	-0.604	-0.016
	SAGE-10	158.245	291.602	-2.974	162.888	50.964	-0.764	-0.017